ESCOLA SUPERIROR D'ENGINYIERIES INDUSTRIALS, AEROESPACIALS I AUDIOVISUALS DE TERRASSA


# Study of a feasible solution for a specific mission with an unmanned air vehicle (UAV/RPAS)

## Attachments

Grau en Vehicles Aeroespacials

Author

**Xavier Vidal Pedrola**

Director

**Aitor Martin Sierra**

Date

10th of June 2017

# Index

## List of figures:

## List of tables:

## List of equations:

# 1. Propulsion system

## 1.1. Engines

### 1.1.1. UL260i

The UL206i is manufactured by ULPower in Belgium[1]. This four-cylinder, four-stroke, horizontally opposed, air-cooled engine, is mainly used on light sport and ultra-light aircrafts. The 95 octane RON is the main fuel. About its performance, this motor has a power output of 71kW (95 hp) at 3300rpm, a weight of 74kg. About the fuel consumption, has a value of 25l/h at 3100rpm. Its specific fuel consumption is 190 g/(kW·h) at 3100rpm. Its price is 15094€.

### 1.1.2. UL350iS

The UL350iS is also manufactured by ULPower in Belgium[2]. This four cylinder, four-stroke, horizontally-opposed, air-cooled, direct drive engine is mainly used on light sport, ultra-light and homebuilt aircrafts. The regular unleaded gasoline is the main fuel, minimum 95 Octane RON. Despite the fact that AVGAS 100 LL can also be used, it is not recommended by the manufacturer. When it comes to its performance, this motor has a power output of 98kW (130 hp) at 3300rpm, a weight of 78.4kg. Talking about the fuel consumption and specific fuel consumption, has a value of 23l/h and 160 g/(kW·h) at 2200rpm, respectively. Has a price of 20140€.

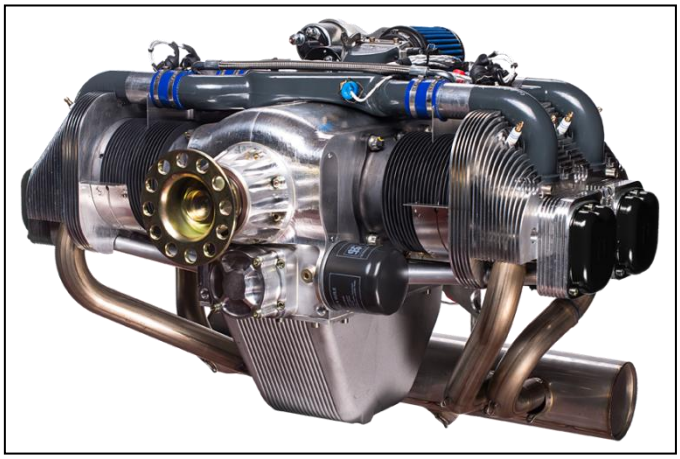

*Figure 1: UL35iS piston engine.*

### 1.1.3. Rotax 912 A

The Rotax 912 is an engine manufactured by the Austrian company called Rotax[3]. It is a horizontally opposed four-cylinder, four-stroke, air and water-cooled, with gear reduction engine commonly used on certified aircraft, light sport aircraft, ultra-light aircraft and unmanned aerial vehicles., Rotax produced the number 50000$^{th}$ 912 series engine in the year 2014, celebrating its big success in the aircraft industry. Its common fuel is the unleaded petrol 90 Octane RON or higher. Has a total weight of 60kg including the fuel pump, air filters, and electric starter and oil systems. Moving on into performance data, has an specific fuel consumption of 280g/(kW·h) at 5500rpm and a power output of 59.6kW (79.9hp) at 5800rpm. Has a price of 18185€.


*Figure 2: Rotax 912 installation on an aircraft.*

## 1.2. Engine selection

Due to the fact that there is more than one possible engine and there is a lot of parameters that may have an impact on the UAV design or its price, one reliable and balanced method has to be selected in order to choose the proper engine that fulfils our conditions and expectations.

The method chosen when one option has to be selected over the others in the whole project is the OWA method.

The parameters evaluated in this OWA are:

- **Minimizing the weight.** Since the engine is placed at the end of the fuselage, putting too much weigh may result in some structural problems.
- **Maximizing the power output.** The power output is an important parameter due to its importance during the takeoff.
- **Minimizing Fuel consumption.** Since the long endurance that our UAV has to achieve, minimizing this parameter is extremely important in order to reduce the fuel needed.
- **Minimizing Specific fuel consumption.** Once again, this parameter has a direct impact on the amount of fuel needed to perform long endurance flights.
- **Minimizing Price.** Even though that there is no economic restriction on the project, trying to reduce the price as much as possible is always a goal.

After scaling each parameter in a scale of 1 to 3 and giving the personal weight on each parameter, the table obtained is:

| | | UL260i | | UL350iS | | Rotax 912 | |
|---|---|---|---|---|---|---|---|
| | **g** | **p** | **p·g** | **p** | **p·g** | **p** | **p·g** |
| **Weight** | 7 | 1,56 | 10,92 | 1 | 7 | 3 | 21 |
| **Power** | 7,5 | 1,57 | 11,775 | 3 | 22,5 | 1 | 7,5 |
| **Fuel con.** | 8 | 1 | 8 | 1,4 | 11,2 | 3 | 24 |
| **Specific fuel con.** | 9 | 1,33 | 11,97 | 3 | 27 | 1 | 9 |
| **Engine Price** | 5,5 | 3 | 16,5 | 1 | 5,5 | 1,77 | 9,735 |
| **SUM** | 37 | | 59,165 | | 73,2 | | 71,235 |
| **OWA** | | | 0,533 | | 0,659 | | 0,642 |

*Table 1: OWA method for engine selection.*

The engine that gets the highest score using the OWA method is the UL350iS followed by the Rotax 912 A and leaving the last position to UL260i.

Each parameter is given a subjective value between 0 and 10, depending on the importance and relevance that it may have on the UAV according to our judgement. The value p goes from 1 to 3 and it is used to escalate each

parameter studied in the OWA. The value 3 is given to the engine fulfils our requirements the most, and the 1 is given to the worst engine.

# 2. Aerodynamics

## 2.1. Configuration of the aircraft

The first step is to make some decisions about the general shape and structure of the plane:

- Medium-low wing: Due to the fact that there is no need of a big cabin in the body of the plane, the low wing is not a viable option. The high wing has been considered because of the fact that it gives a higher aerodynamic efficiency. However, the downside of the landing gear and the additional difficulties that it gives to the wing-fuselage joint made the high wing configuration a less efficient option. Thus, the medium-low wing has been chosen by elimination process.
- Cruciform tail (A-2): The cruciform tail has been selected by a procedure of elimination. The T-tail (A-3) was not a viable option because of the high structural stress that suffers the root, where the engine is placed. The conventional configuration (A-1) was not good decision either due to the fact that the engine is placed on the trailing edge of the fuselage. The twin vertical tails, the butterfly tail and V-tail have been discarded due to the structural complexity and the difficulties of their aerodynamic analysis.

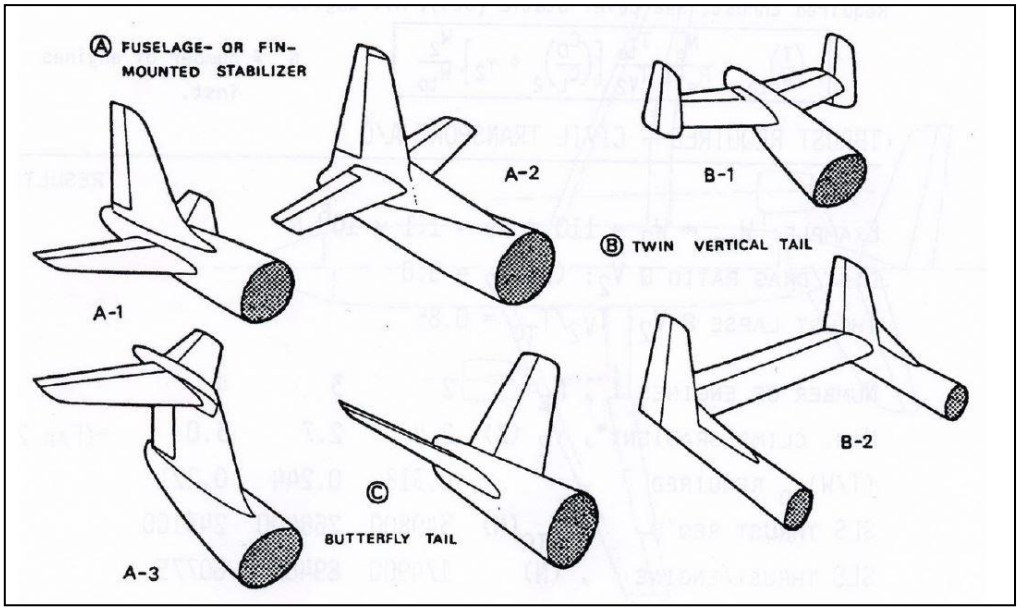


*Figure 3: Tail configurations.*

## 2.2. Reynolds Number

The Reynolds number (Re) is a non-dimensional parameter based on a first estimation of the wing dimensions and the height of flight. To calculate the Reynolds number, we will use the following equation:

$$Re = \frac{\rho \cdot v_s \cdot c}{\mu} \quad (1)$$

Where $\rho$ is the density of the fluid in kg/m$^3$, $v_s$ is the characteristic speed of the fluid in m/s, $c$ is the chord of the airfoil and $\mu$ is the viscosity of the fluid in N*s/m$^2$. Replacing the numbers on the equation mentioned above:

$$Re = \frac{0.9568 \cdot 50 \cdot 2}{1.73 \cdot 10^{-5}} = 5.5315 \cdot 10^6$$

The number of Reynolds obtained is similar to the light aircraft due to the fact that our UAV uses a low speed, a medium chord and flights at low height. As a result of this high number obtained, the viscous forces are going to be neglected during the aerodynamic analysis.

## 2.3. Wing

### 2.3.1. Airfoil

#### *2.3.1.1. Airfoils list*

The list of airfoils studied with the XFLR5 software the following:

| | |
|---|---|
| Airfoils | AG35 |
| | AH 95 -160 |
| | Clark Y |
| | FX 60-100 |
| | FX 76-MP-120 |
| | N-11 |
| | NACA 4415 |
| | NACA 6412 |
| | NASA NLF1015 |
| | SG6043 |

*Table 2: Airfoils list.*

*2.3.1.2. Airfoils analysis conditions*

After completing the list of airfoils, the next step is to aerodynamically compare the airfoils. To do that, after searching and importing each airfoil coordinates[4], a model is created in XFLR5 software using the same flight conditions and wing and tail configuration. Those conditions and configurations are the following:

| | | |
|---|---|---|
| Wing configuration | Span (m) | 7 |
| | Chord (m) | 2.25 |
| | Dihedral (º) | 0 |
| | Twist (º) | 0 |
| | Tilt angle (º) | 1 |
| Tail configuration | Distance to wing (m) | 2.5 |
| | Span (m) | 5 |
| | Chord (m) | 1.25 |
| | Twist (º) | 0 |
| | Tilt angle (º) | -2 |
| | Airfoil | NACA 0012 |
| UAV | Weight (Kg) | 450 |
| | Centre of mass position x axis (m) | -0.5 |
| Atmosphere conditions | Density (kg/m$^3$) | 1.225 |

*Table 3: Aerodynamic analysis conditions and configurations.*

*2.3.1.3. Airfoils OWA parameters*

Before using the OWA method to decide which airfoil will be chosen, a list of each airfoil with his parameters will be done to ease the OWA process and understanding.

Those parameters are:

- Minimum thickness.
- Minimum $v_{stall}$.
- Maximum efficiency.

| Airfoil name | Max. Thickness (%) | $V_{stall}$ (m/s) | Max. Efficiency |
|---|---|---|---|
| AG35 | 8.72 | 19.28 | 42.8 |
| AH 95 -160 | 16.0 | 18.82 | 33 |
| Clark Y | 11.71 | 20.01 | 49.5 |
| FX 60-100 | 9.9 | 19.08 | 37 |
| FX 76-MP-120 | 12.11 | 17.89 | 25.5 |
| N-11 | 10.93 | 18.75 | 33 |
| NACA 4415 | 14.99 | 19.17 | 39 |
| NACA 6412 | 12.04 | 18.69 | 31 |
| NASA NLF1015 | 14.99 | 18.43 | 27.5 |
| SG6043 | 10.01 | 18.41 | 27.5 |

*Table 4: OWA parameters of each airfoil.*

#### *2.3.1.4. Airfoil's OWA*

Due to the fact that the OWA table is too big because there are a lot of airfoils to compare, only the best four will be shown.

| | | AG35 | | Clark Y | | FX 60-100 | | N-11 | |
|---|---|---|---|---|---|---|---|---|---|
| | **g** | **p** | **p·g** | **p** | **p·g** | **p** | **p·g** | **p** | **p·g** |
| **Thickness** | 1 | 10,00 | 10,00 | 6,32 | 6,32 | 8,35 | 8,35 | 7,08 | 7,08 |
| **$V_{stall}$** | 2 | 2,86 | 5,73 | 1,00 | 2,00 | 3,71 | 7,43 | 5,11 | 10,23 |
| **Efficiency** | 3 | 7,48 | 22,44 | 10,00 | 30,00 | 5,31 | 15,93 | 3,81 | 11,43 |
| **SUM** | 6 | | 38,17 | | 38,32 | | 31,71 | | 28,73 |
| **OWA** | | | 0,636 | | 0,639 | | 0,528 | | 0,479 |

*Table 5: OWA results for airfoils choice.*

The airfoil that has the highest OWA points according to our criteria is Clark Y. The importance given to the parameters is represented by the value of "g". Maximum efficiency is given the most importance, followed by $v_{stall}$ and ending with the maximum thickness. The parameter p escalates the values of each airfoil giving form 1 to 10.

### 2.3.2. Wing shape

#### *2.3.2.1. Taper ratio*

The taper ratio is defined as the chord in the root divided by the chord on the root:

$$\lambda = \frac{c_{tip}}{c_{root}} \quad (2)$$

The taper ratio of 1 is a rectangular wing, the simplest structure and thus, the most weight saver. However, after aerodynamically analysing the plane, the rectangular wing has been found to be less efficient than the wing with a lower taper ratio. Since aerodynamic efficiency is one of the main goals due to the high endurance of the UAV, the rectangular wing shape has been rejected.

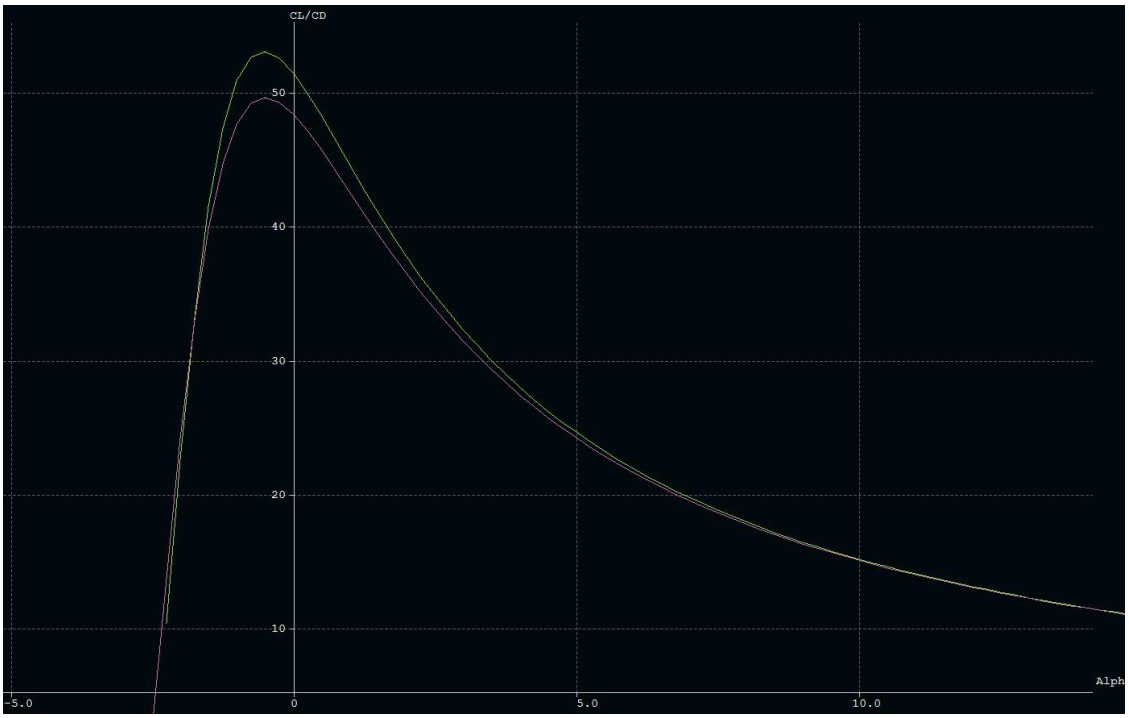


*Figure 4: Comparison rectangular wing (purple) vs taper ratio wing (green).*

As the graph shows, the taper ratio wing offers a slightly better aerodynamic performance due to the reduction on the induced drag generated.

*2.3.2.2. Sweep angle*

In subsonic flight, the only main advantage resides in stability purposes. However, our aircraft is provided with a tail in order to fulfil that role. Furthermore, when it comes to efficiency, an excess of sweep angle will result in an increase of the induced drag. Because of those two reasons, the sweep angle has been chosen in order to reduce the structural stress produced by the bending and torsion moment due to the aerodynamic loads.

*2.3.2.3. Twist*

Depending on the wing shape used, the stall effects starts in different points of the wing. The worst scenario happens with the elliptical configuration. As is it shown on the figure below, the elliptical shape suffers the stall effects in the whole wing at the same time, causing a state called “deep stall”, losing the whole lift and manoeuvrability of the plane on the control surfaces, making the aircraft impossible to control. The perfect situation is the rectangular wing due to the fact that starting the stall on the empennage will allow the pilot to still have control over the ailerons usually located on the end of the wing.

In our case, the stall starts at the tip of the wing, in order to move the stall effect closer to the fuselage, some geometrical twist will be added.

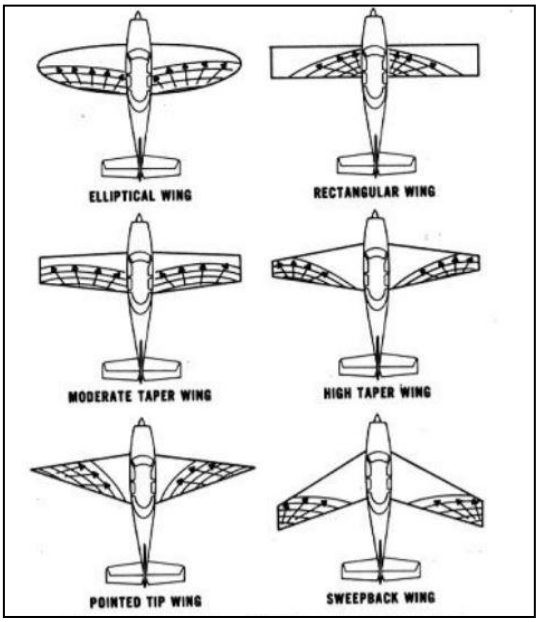


*Figure 5: Stall effect depending on wing shape.*

*2.3.2.4. Dihedral*

Despite the fact that adding a dihedral will result in an increase of the aerodynamic efficiency, since the main span has a break due to the taper ratio of the wing, the dihedral may result on a harder structural problem. Since the final weight is also a big concern, the dihedral is going to be neglected to reduce final costs and weights.

### 2.3.3. Control surfaces

The area of the aileron has been calculated using the theory and the example found in an article[5].

Since the process may require more than one iteration, the software used in order to solve the calculations is Microsoft Excel.

The process consists of choosing the time required to perform a bank angle according to some experimental data. Afterwards, obtain and estimate some geometrical parameters such as the inwards and outwards aileron position, the max aileron deflection, etc. Finally, after calculating the time required with that configuration and comparing it with the time required from the experimental data, a decision whether the aileron is suitable or not is made.

The known inputs of the program are:

- Wing Area (S).
- Wingspan (b).
- Root chord ($c_r$).
- Tip chord ($c_p$).
- Vertical Stabilizer Area ($S_v$).
- Horizontal Stabilizer Area ($S_h$).
- Stall speed ($v_{stall}$).
- $Cl_{alpha}$. The slope of CL/alpha polar.
- $I_{xx}$. Plane inertia on the X axis.

The estimated parameters are:

- $Y_{inwards}$. Starting aileron wingspan position.
- $Y_{outwards}$. Ending aileron wingspan position.
- Maximum aileron deflection.
- Aileron chord.

After calculating and optimizing the aileron geometry and configuration, an extended analysis has been made to obtain the time required to achieve any time angle between 0º and 40º. Both program outputs are shown in the report.

### 2.3.4. High lift devices

The high-lift devices can be divided into two groups: leading edge and trailing edge devices. Each category offers a wide variety of options:

Starting with the leading edge, the devices mainly used are:

- Fixed slot.
- Two position slat (takeoff-landing).
- Three positions slat (cruise-takeoff-lading).
- Leading edge flap.

The following figure shows some of the devices mentioned above:

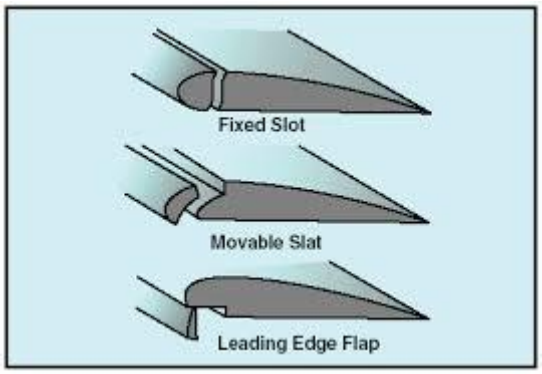


*Figure 6: High lift devices used on the leading edge.*

Moving on to the trailing edge:

- Plain flap.
- Split flap.
- Flap Fowler.
- Single slotted flap.
- Double slotted flap

The list of flaps shown above are the simple ones and used as a base to design more complex and sophisticated ones, such as the Zap-Flap, the Junkers flap or the Gouge flap. The following image shows the ones mentioned on the list:

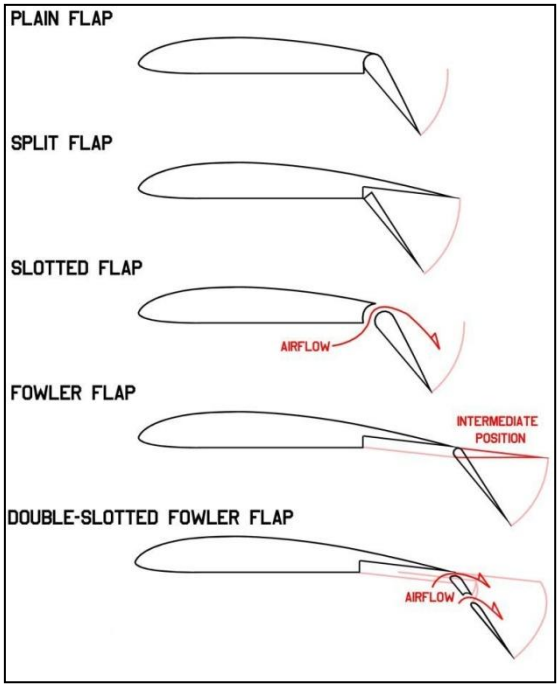


*Figure 7: High lift devices used on the trailing edge of the wing.*

Further information about the high lift devices can be found on books that specifically talk about that matter[6,7].

## 2.4. Tail

### 2.4.1. Horizontal stabilizer

#### *2.4.1.1. Area*

Since the main purpose of the stabilizer is to counter the moment produced by the wing, there is a tight relation between both devices. In order to determine the surface of the horizontal stabilizer, the design procedure followed is by using the horizontal tail coefficient volume $C_{(\mathrm{H})}$. That non-dimensional parameter reflects the effectiveness of the horizontal stabiliser according to the moment created by the area of the tail.

The equation that defines the horizontal tail volume is:

$$C_{\mathrm{H}} = \frac{S_H \cdot l_H}{S_w \cdot c_{\mathrm{mac}}} \qquad (3)$$

Where:

- $S_H$: Horizontal stabilizer area.
- $l_H$: Elevator lever arm.
- $S_w$: Wing area.
- $c_{\text{mac}}$: Mean aerodynamic chord of the wing.

Before solving the equation for $S_H$, one more estimation is needed in order to know the value of all the other parameters shown in the equation, the value of $C_{\text{H}}$ . The table of this parameter can be estimated by experimental data, as it is shown in the following table[8]:

| | Horizontal $c_{HT}$ |
|---|---|
| Sailplane | 0.50 |
| Homebuilt | 0.50 |
| General aviation—single engine | 0.70 |
| General aviation—twin engine | 0.80 |
| Agricultural | 0.50 |
| Twin turboprop | 0.90 |
| Flying boat | 0.70 |
| Jet trainer | 0.70 |
| Jet fighter | 0.40 |
| Military cargo/bomber | 1.00 |
| Jet transport | 1.00 |

*Figure 8: Estimated horizontal stabilizer volume for each type of aircraft.*

Thus, our UAV can be placed as a homebuilt aircrafts due to its flight conditions, weight distribution and wing configuration.

Once all the parameters are valued, the next step is to solve equation (3).

$$S_H = \frac{C_{\text{H}} \cdot S_w \cdot c_{\text{mac}}}{l_H} = \frac{0.5 \cdot \ 11.25 \cdot 1.56}{2.31} = 3.79\ m^2$$

The value will be rounded to 4 $m^2$.

*2.4.1.2. Aerodynamic parameters*

After calculating the area needed, some other parameters that affect mainly the aerodynamic performance of the stabilizer have to be set. The parameters obtained can be summarized as[9]:

Aspect ratio ($AR_h$): Has the same definition as in the wing. The value of that parameter has to be lower than the aspect ratio of the wing, the main lift device. The reason is that the deflection of the elevator creates a large bending moment at the root. Thus, reducing that value will result on a lower bending stress.

Taper ratio ($\lambda_h$): That value is obtained by dividing the chord at the tip with the chord at the root. This parameter has a typical value between 0.5 and 1. The main motivation behind this parameter is to lower the tail weight.

Sweep angle: The sweep angle of the horizontal tail mainly influences the aircraft longitudinal and lateral stability and control and the tail aerodynamic efficiency. The value given to the sweep angle is approximately the same as given for the wing.

*2.4.1.3. Height*

The height of the horizontal tail relative to the wing is an important parameter. When it comes to the tail installation, it can only be placed in the fuselage aft section or at the vertical tail. Unlike the wing location, there is no such a thing as the low tail, mid tail or high tail. Instead, the tail vertical position implies a conventional tail if it is low located, a cruciform tail if it is mid located and T-tail in case of high height.

The best way to calculate the height position is by some software able to perform aerodynamic analysis due to the fact that the trail effectiveness is influenced by many elements, such as the wing, engine and fuselage.

The main problem relating the wing and the horizontal stabilizer is called “deep stall”. The following figure graphically explains the problem[9].

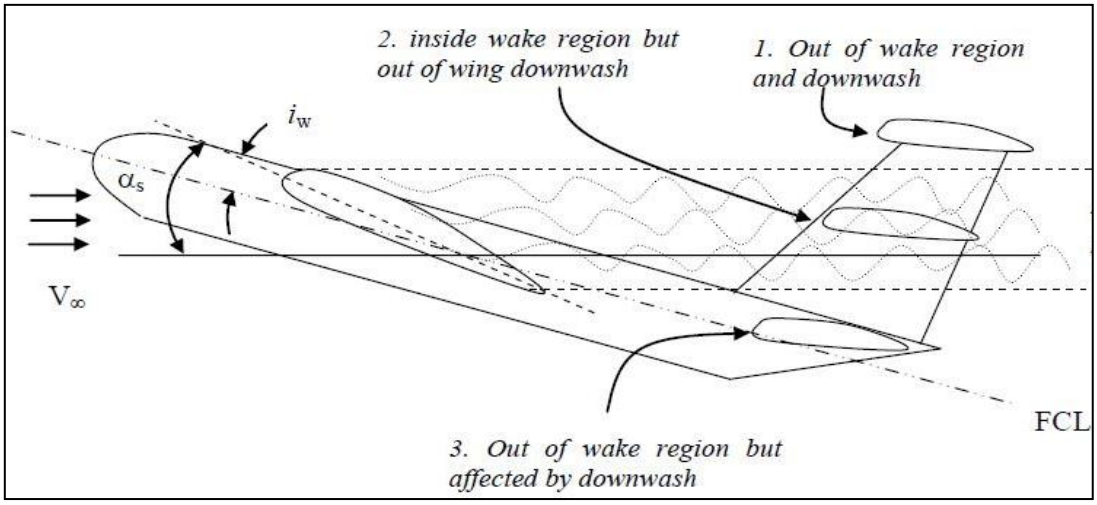


*Figure 9: Regions defined by the deep stall effect.*

The region behind the wing is in the region called deep stall region. Due to the turbulent flux created by the wing, the wing is unable to generate any aerodynamic force. Making the aircraft impossible to control and stabilize unless the tail regains its free clean air flux. According to the picture, the best position to place the tail in this plane is the T-tail due to the fact that it is not affected by the wake region neither the downwash. On the other hand, the conventional tail is also a possible solution but the tail will lose effectiveness due to the wing downwash.

#### *2.4.1.4. Elevator*

In order to design the control surfaces of the horizontal stabilizer, the theory and example found in an article has been followed[10].

The software used in order to solve the calculations is Microsoft excel due to the need of a software able to ease the iteration process required.

Before starting to solve the elevator problem, some other points have to be fully defined and completed in order to obtain a more accurate solution by reducing the number of estimations. Some of those tasks that must be performed before the elevator are: aircraft general dimensioning and weight distribution, aerodynamic and geometric horizontal stabilizer configuration and landing gear positioning.

The main scheme used in order to solve the control surface problem is:

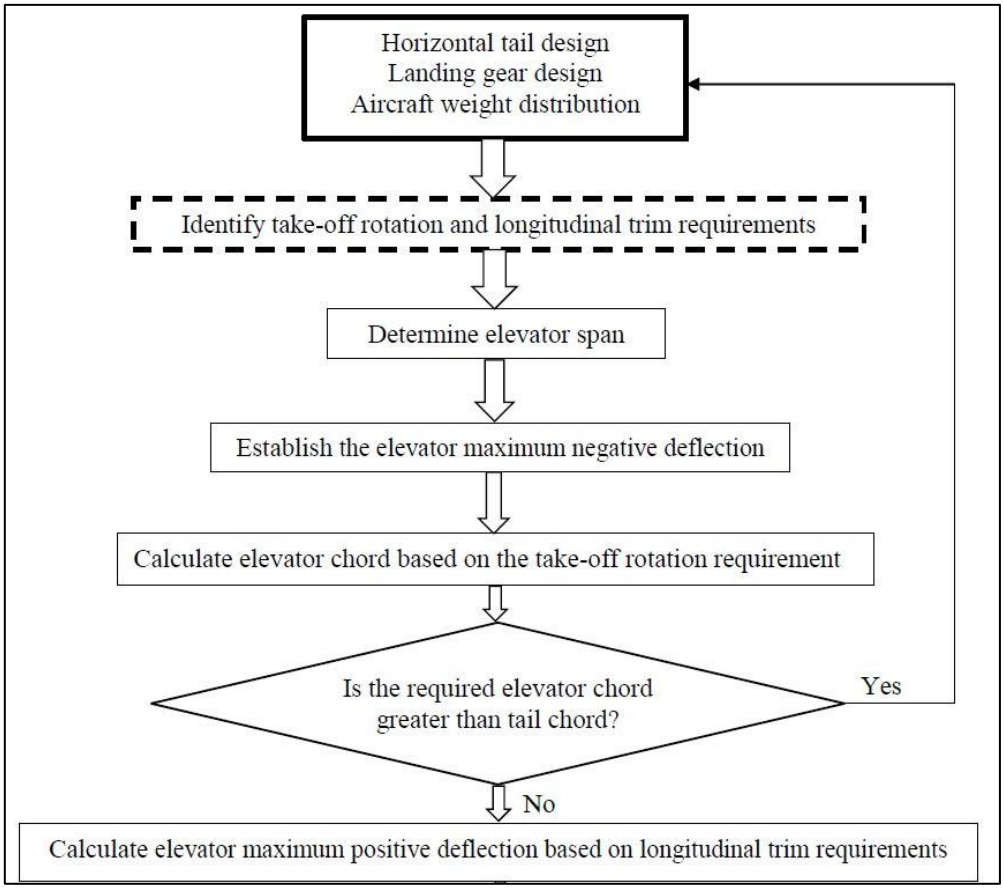


*Figure 10: Diagram used during the elevator calculations.*

As for the ailerons, the resolution uses some known parameters and some estimated parameters that should be optimized by iteration method in order to obtain the most accurate solution. In order to completely define the elevator surface, four parameters have to be valued:

- Elevator area ($S_E$).
- Elevator chord ($C_E$).
- Elevator span ($b_E$).
- Maximum elevator deflection ($\pm\delta_{Emax}$).

Generally, those values are expressed in terms of the horizontal stabilizer. Those parameters are highly interrelated and its range of value depends mainly on the horizontal tail dimensions. Except for the elevator deflection, that generally cannot be higher than 20º or lower than -20º due to the flow separation over the tail, reducing the pitch control effectiveness.

### 2.4.2. Vertical stabilizer

#### *2.4.2.1. Area*

The method used in order to calculate the area of the vertical stabilizer is making use of the vertical coefficient volume ($\bar{v}_v$). The equation that relates the coefficient volume and the area is the following:

$$\bar{v}_v = \frac{l_v \cdot S_v}{b \cdot S_w} \tag{4}$$

Solving the equation for $S_v$:

$$S_v = \frac{\bar{v}_v \cdot b \cdot S_w}{l_v} \tag{5}$$

Where:

- $l_v$: Vertical tail moment arm.
- $b$: Wingspan.
- $S_w$: Wing area.

The value of $\bar{v}_v$ can be estimated by semblance with other planes. Our UAV can be compared with a single prop driven engine or a home-build aircraft due to the flight conditions, weight distribution and wing configurations. Both aircrafts have a vertical tail coefficient volume of 0.04[9].

Replacing the parameters for our UAV values, the following area is obtained:

$$S_v = \frac{0.04 \cdot 7.5 \cdot 11.25}{2.75} = 1.25\ m^2$$

#### *2.4.2.2. Aerodynamic parameters*

Once the surface is known, the optimization of the aerodynamic performance of the vertical stabilizer becomes the next goal. In order to choose a viable shape and aerodynamic parameters, some research has been done[6].

Aspect ratio ($AR_v$): The values of the aspect ratio range from 1 to 2 approximately. Some of the advantages and disadvantages of choosing a high aspect ratio are:

1) A high tail aspect ratio weakens the aircraft lateral control, since the vertical tail mass moment of inertia in the x-axis is increased.
2) A high aspect ratio has a longer yawing moment arm compared with a lower ratio. Thus, the directional control is increased.
3) A higher aspect ratio increases the bending moment and bending stress. Hence, the vertical tail root has to be stronger, leading to a higher structural weight.
4) A high aspect ratio is longitudinally destabilizing due to the vertical drag, creating a nose-up pitch moment.
5) As the aspect ratio increases, the vertical tail induced drag is also increased.
6) A high aspect ratio is more aerodynamic efficient than a lower one due to the vertical tail tip effect.

Taper ratio ($\lambda_v$): Has a value range between 0.6 and 1. The main purposes of the taper ratio are:

1) To reduce the bending stress on the vertical root.
2) To provide the vertical tail with a sweep angle.

An increase of the taper ratio will result in a reduction of the yawning moment. Thus, the directional control of the UAV is reduced. Furthermore, a high value of taper ratio also reduces the lateral stability of the aircraft.

Sweep angle: The sweep angle should not exceed 20º. A large sweep angle increases the yawing moment arm whereas it weakens the aircraft directional stability due to an increase of the moment inertia on the z-axis.

Dihedral angle: Since the aircraft symmetry required on x-z plane, an airplane with one vertical tail is cannot have any dihedral angle. However, if the aircraft has twin vertical tails, the dihedral angle has positive contributing on the lateral control.

*2.4.2.3. Dorsal fin*

The dorsal fin is located in front of the vertical stabilizer; connected with the fuselage.


*Figure 11: Dorsal wing on a commercial aircraft.*

The benefit that a dorsal fin offers is an increase of the vertical stabiliser efficiency at high angles of sideslip angle due to the formation of early vortexes. Those vortexes will increase the stall region of the tail, allowing the plane to land or takeoff during higher sideslip angles as it is shown on the figure above[11]:

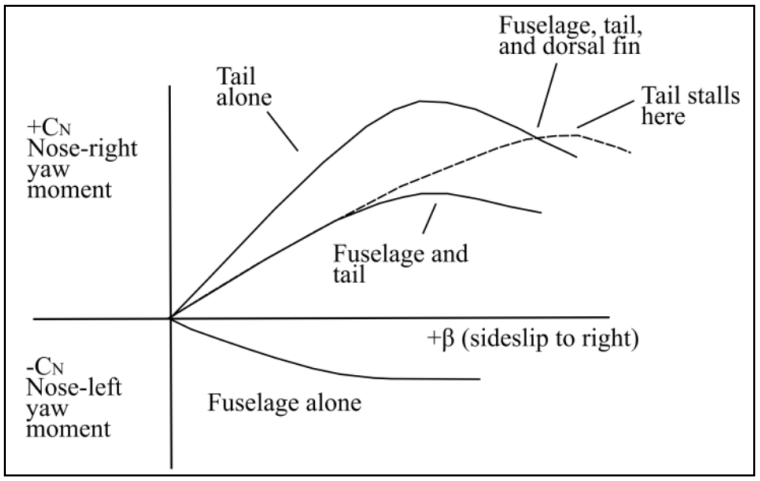


*Figure 12: Tail stalls depending on the elements studied.*

## 2.5. Performance

The following section will calculate assuming some simplifications in order to be able to obtain an analytical solution of the Breguet equations and the takeoff and landing operations.

### 2.5.1. Breguet equations (cruise conditions)

The next calculation is the range and endurance of our UAV integrating the Breguet equations for a piston engine. Those equations are the same as used on a turboprop airplane since the engine outputs are measured in terms of power[12].

For a maximum endurance, the fuel consumed per unit time must be determined, so minimizing the following equation is a priority:

$$\frac{d\,W_f}{d\,t} => \frac{N\,fuel}{sec} \tag{6}$$

To get the maximum range, our interest is placed in determining the fuel consumed per unit distance:

$$\frac{d\,W_f}{d\,S} => \frac{N\,fuel}{m} \tag{7}$$

The fuel consumption for the engines whose output is measured in terms of power is called power specific fuel consumption (PSFC) and it is defined as:

$$c_p = \frac{\text{N fuel}}{\text{watts} \cdot \text{hour}} \tag{8}$$

In order to solve the equation, the quasi-level flight conditions must be applied. That means equilibrium of forces during the whole flight. (L=W and T=D). Also, the level or quasi level flight implies the relation between the engine shaft power and the propulsive efficiency:

$$P_{av} = P_s \cdot \eta_p = D \cdot v \qquad => \qquad P_s = \frac{Dv}{\eta_p} \tag{9}$$

Now, combining the equation number (6), (8) and (9), the following endurance equation is obtained:

$$\frac{d\,W_f}{d\,t} = c_p \cdot P_{av} = \frac{c_p \cdot P_s}{\eta_p} = \frac{c_p \cdot D \cdot v}{\eta_p} \tag{10}$$

Repeating the same process for the range equation:

$$\frac{d\,W_f}{d\,S} = \frac{d\,W_f/d\,t}{d\,S/d\,t} = \frac{c_p \cdot D \cdot v}{\eta_p \cdot v} = \frac{c_p \cdot D}{\eta_p} \tag{11}$$

Before moving into solving the integral, some corrections will be done. The weight reference is going to be placed on the aircraft weight instead of the fuel weight. Furthermore, the following hypothesis may be considered before solving the integral equation:

- $c_p$ is constant during the whole flight.
- $\eta_p$ remains constant all the flight.
- Flight under constant angle of attack
- The air speed value does not change along the path.

$$E = -\int_{W_1}^{W_2} \frac{\eta_p}{c_p} \frac{1}{v} \frac{C_L}{C_D} \frac{dW}{W} \tag{12}$$

Now, solving the integral and using the hypothesis shown above:

$$E = \frac{\eta_p}{c_p} \frac{1}{v} \frac{C_L}{C_D} ln \frac{W_1}{W_2} \tag{13}$$

Five factors have a direct impact if we want to increase the endurance of an aircraft:

1. The higher the $\eta_p$ of the motor, the better.
2. Try to minimise the $c_p$ of the motor used on the plane or UAV.
3. Reducing the flying speed will increase our endurance.
4. Try to maximise the aerodynamic efficiency of the aircraft.
5. A large amount of fuel.

Moving on to range calculations, using equation (7) and considering T=D and L=W:

$$\mathrm{R} = -\int_{W_1}^{W_2} \frac{\eta_p}{c_p} \frac{C_L}{C_D} \frac{dW}{W} \tag{14}$$

Solving the integral by applying the same hypothesis used on the endurance Breguet equation:

$$\mathrm{R} = \frac{\eta_p}{c_p} \frac{C_L}{C_D} ln \frac{W_1}{W_2} \tag{15}$$

In order to solve equation (13) and (15), a Matlab little script has been done to solve the equations once all the parameters are known. Due to the fact that the parameters that effect both equations depend on the wing configuration, the tail, the propeller and the engine, the script has been updated and corrected each time that one modification affecting one of the elements mentioned above has been done.

### 2.5.2. Takeoff

The takeoff procedure it is on some hypothesis to ease the calculations[13]. Following the instructions given by the author, the take off distance can be divided into:

- Roll ground distance. ($S_g$)
- Air phase distance. ($S_a$)

The equations used in order to relate that distance with the engine, aerodynamic and ground parameters are:

$$S_g = \frac{W \cdot v_{t.o}^2}{2g[F - D - \mu(W - L)]_{avg}} \quad (16)$$

$$S_a = \frac{W\frac{(v_{50}^2 - v_{t.o}^2)}{2g} + 15}{(F - D)_{avg}} \quad (17)$$

Where:

- W: Weight of the aircraft on takeoff.
- $V_{t.o}$: Velocity of the aircraft during the take off. Its calculated as:

$$v_{t.o} = 1.1 \cdot v_{stall} = 1.1 \cdot \sqrt{\frac{2W}{\rho S CL_{max}}}$$

- $CL_{max}$: Maximum lift coefficient at take off.
- $g$: Earth gravity.
- $F$: Average thrust of the aircraft.
- $D$: Average aerodynamic resistance.
- $L$: Average aerodynamic lift produced.
- $\mu$: Runway friction coefficient.

- $v_{50}$: Velocity of the aircraft when reaching a distance of 50 feet between the plane and the ground. Is defined as:

$$v_{50} = 1.3 \cdot v_{stall}$$

After replacing the values of each parameter and obtaining the ground and air distance required, a factor of 1.15 is multiplied by the length in order to fulfil the ICAO requirements.

### 2.5.3. Landing

The landing distance follows the same scheme used for the take off performance and the theory and equations obtained are taken from the same book[13].

The landing distance is divided by the air distance ($S_a$) and the ground distance ($S_g$) too. The equations used are:

$$S_a = \frac{W_L \frac{(v_{TD}^2 - v_{50}^2)}{2g} - 15}{(F - D)_{avg}} \quad (18)$$

$$S_g = \frac{W_L \cdot v_{TD}^2}{2g[F - D - \mu(W_L - L)]_{avg}} \quad (19)$$

Where:

- $W_L$: Aircraft weight when landing.
- $v_{TD}$: Velocity when touching down. Is defined as:

$$v_{TD} = 0.8 \cdot v_{stall}$$

- $v_{50}$: Velocity of the aircraft when reaching a distance of 50 feet between the plane and the ground. Is defined as:

$$v_{50} = 1.3 \cdot v_{stall}$$

# 3. Structures

## 3.1. Weight calculations

### 3.1.1. Takeoff weight

The takeoff weight is extremely hard to value with an extremely high accuracy, thus, the method used in order to determine that parameter is by an iterative process. That means that the value was first estimated and has been changed along the time as the project was evolving and taking form.

The first value was estimated by comparing the ratio of payload/OEW of similar aircrafts and the value of the endurance/FW of the aircrafts with a comparable wing configuration and endurance. The first MTOW estimated was between 390kg and 410kg.

The final MTOW has been set as 460kg.

### 3.1.2. Payload weight

The payload calculation is the sum of each device's weight used in order to whether the drone position (GPS) or the position of any shipwreck (thermal and optical camera, radar ...).

| | |
|---|---|
| Thermal and optical camera (kg) | 27 |
| Maritime radar (kg) | 10 |
| Tracking system (kg) | 0,5 |
| AIS receiver (kg) | 0,28 |
| Satellite link system (kg) | 8 |
| **TOTAL WEIGHT (kg)** | **45,78** |

*Table 6: Payload's weight.*

### 3.1.3. Fuel weight

The maximum fuel weight in order to obtain the maximum endurance can be computed as it follows.

Taking the fuel consumption per hour at 2100 rpm provided by the manufacturer[2] ($F_{cons}$), knowing the endurance required ($t$) and the density of the AVGAS ($\rho_{fuel}$), the following equation can be solved:

$$FW = F_{cons} \cdot t \cdot \rho_{fuel} \tag{20}$$

$$FW = 22.5 \cdot 13 \cdot 0.72 = 210\ kg$$

### 3.1.4. Operational empty weight

The operational empty weight can be calculated using the following equation once the other three weights are known:

$$OEM = MTOW - FW - PL \tag{21}$$
$$OEM = 460 - 210 - 40 = 210\ kg$$

## 3.2. Centre of gravity

Before stating which distances are being used for each airplane device, the origin of the reference system must be defined.

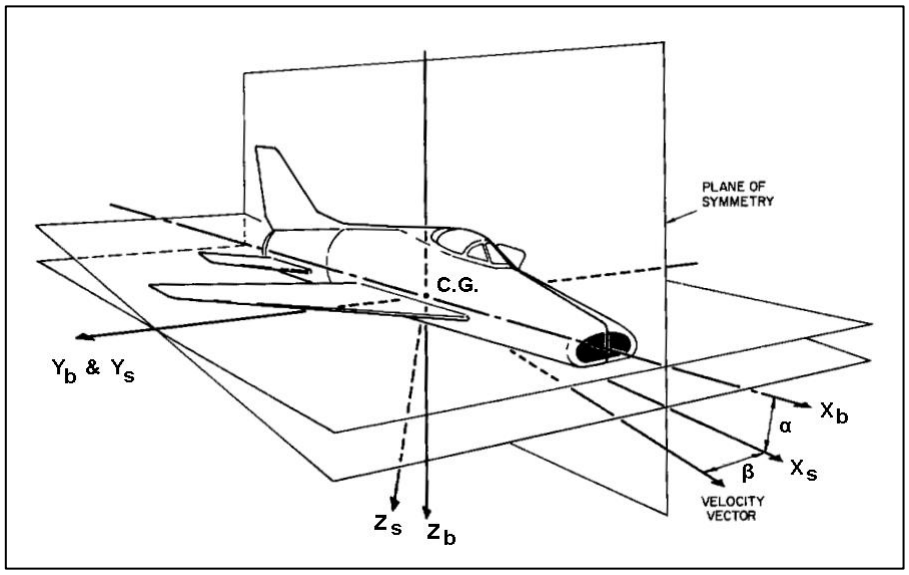


*Figure 13: Airplane body axis and stability axis.*

The direction of the axis is the same as defined in the figure shown above. However, since the centre of gravity (CG) is the point that we are looking for, the reference point used in order to calculate the CG is defined in the same axis but is placed in the nose of the UAV, which is a known point that will allow us to procedure with the centre of gravity calculations. In order to simplify and ease the calculations, the direction of the x-axis has been switch to avoid the use of the minus sign in front of every position.

### 3.2.1. X-axis

The distance estimated for each device and its weight is collected on the following table:

| Aircraft component | Weight (kg) | Distance (m) |
|---|---|---|
| Wing | 40 | 4.5 |
| Tail | 20 | 7.1 |
| Main landing gear | 25 | 4.55 |
| Leading edge landing gear | 10 | 1.2 |
| Engine | 78 | 6.9 |
| Propeller | 12 | 7.5 |
| Payload | 45 | 0.2 |
| Fuselage A | 115 | 1.5 |
| Fuselage B | 70 | 3.5 |
| Fuselage C | 35 | 5.5 |

*Table 7: Mass and coordinate of the UAV's components on the x-axis.*

The formula used to compute the final x coordinate position is:

$$x_{cg} = \frac{\sum_{i=1}^{n} m_i \cdot x_{cg_i}}{\sum_{i=1}^{n} m_i} \quad (22)$$

Replacing the values and solving the equation:

$$x_{cg} = 3.735\ m$$

### 3.2.2. Y-axis

Since the centre of gravity on the y-axis is placed on our reference, the x-z plane:

$$y_{cg} = 0m$$

### 3.2.3. Z-axis

Moving on to the z-axis, as the x-y plane is placed in the symmetry of the plane, the distances on the z-axis are rated positive if the height is above and negative if the element is under that plane of symmetry. The elements rated with a distance equal to zero have their centre of gravity on the plane of symmetry.

The weight of the elements remains the same. Thus, the only parameters needed are the distances.

| Aircraft component | Distance (m) |
|---|---|
| Wing | -0.4 |
| Tail | 0.6 |
| Main landing gear | -0.6 |
| Leading edge landing gear | -0.6 |
| Engine | 0.4 |
| Propeller | 0.4 |
| Payload | 0 |
| Fuselage A | 0 |
| Fuselage B | 0 |
| Fuselage C | 0 |

*Table 8: Coordinate of the UAV's components on the z-axis.*

Applying the same formula used on the x-axis:

$$z_{cg} = \frac{\sum_{i=1}^{n} m_i \cdot z_{cg_i}}{\sum_{i=1}^{n} m_i}$$

The value obtained is:

$$z_{cg} = 0.024m$$

## 3.3. UAV Inertias

The method used to calculate the inertias of the drone, are based on a theory made by Jan Roskam[14]. This method makes the assumption that inertias can be computed by a parameter called radius of gyration (Rx, Ry, and Rz) specific for each plane. The moments of inertia are given by those equations:

$$I_{xx} = {W(R_x)^2}/{g} \quad (23)$$

$$I_{yy} = {W(R_y)^2}/{g} \quad (24)$$

$$I_{zz} = {W(R_z)^2}/{g} \quad (25)$$

Experimental data has proved that these radiuses of gyration are related with other plane parameters such as the airplane length or the wingspan. Therefore, the equations can be rewritten as:

$$I_{xx} = {b^2 W(\overline{R_x})^2}\Big/{4g} \quad (26)$$

$$I_{yy} = {L^2 W(\overline{R_y})^2}\Big/{4g} \quad (27)$$

$$I_{zz} = {(b+L)^2 W(\overline{R_z})^2}\Big/{16g} \quad (28)$$

Where W is in lbs and L and b are in ft. The next step is to obtain those non-dimensional radiuses of gyration on the Appendix B of [14].

The following parameters are obtained for our plane:

$$\overline{R_x} = 0.268$$

$$\overline{R_y} = 0.360$$

$$\overline{R_z} = 0.420$$

Now solving equations (26), (27) and (28), the following values are obtained:

$$I_{xx} = 464.61\ kg \cdot m^2$$

$$I_{yy} = 730.29\ kg \cdot m^2$$

$$I_{zz} = 1066.30\ kg \cdot m^2$$

## 3.4. Materials

The materials selection is an important point of the project due to the impact that has on the structural calculations. The method used to choose the correct material is by an OWA table. Now that the method has been chosen, the properties that are going to be compared will be chosen:

- **Density**: The relation between weight and volume has to be minimized in order to reduce the final weight of the UAV.

- **Young Modulus**: Is a measure of the stiffness of a solid material. Relates the stress and strain in a material. The higher, the better.
- **Ultimate Tensile Stress (UTS):** This value dictates at which stress the material breaks due to an excessive effort. A higher value means that it can handle higher external loads.
- **Yield tensile stress**: Once one material supper passes this value, it starts to elongate and does not regain its original form even if the external force stops. That permanent deformation is important since it can modify the load distribution, making the structure less effective.
- **Shear strength:** This value shows the strength of the material to transversal forces instead of the normal ones.
- **Elongation at break:** This parameter is expressed in % and shows how much can the material elongate before breaking. It is related with the yield tensile stress and the UTS.

### 3.4.1. Materials studied and properties

The following table sums up all the aluminium that will be studied for the internal structure and their properties:

| MATERIALS | 7075-T6 | 7050-T74 | 2024-T6 | 6063-T6 |
|---|---|---|---|---|
| **Density [kg/m$^3$]** | 2810 | 2830 | 2780 | 2700 |
| **Young's Modulus [GPa]** | 71,7 | 71,7 | 72,4 | 68,9 |
| **Ultimate Tensile Stress [MPa]** | 572 | 524 | 427 | 241 |
| **Yield Tensile Stress [MPa]** | 503 | 469 | 345 | 214 |
| **Shear Strength [MPa]** | 331 | 303 | 283 | 152 |
| **Elongation at break [%]** | 11 | 11 | 9 | 12 |

*Table 9: Materials properties for internal structure.*

All the aluminium alloys physical properties have been taken from the website[15].

Moving on to the skin:

| MATERIALS | 2024-T3 | 6061-T6 | CFRP | 2014-T6 |
|---|---|---|---|---|
| **Density [kg/m3]** | 2780 | 2700 | 1600 | 2800 |
| **Young's Modulus [GPa]** | 73,1 | 68,9 | 70 | 72,4 |
| **Ultimate Tensile Stress [MPa]** | 485 | 310 | 600 | 483 |
| **Yield Tensile Stress [MPa]** | 345 | 276 | 200 | 414 |
| **Shear Strength [MPa]** | 283 | 207 | 90 | 290 |
| **Elongation at break [%]** | 18 | 12 | 0,85 | 13 |

*Table 10: Materials properties for the skin.*

The aluminium data is extracted from [15] whereas the Carbon Fiber Reinforced Polymer is obtained from the datasheet [16].

### 3.4.2. OWA results

Since there are 4 materials, each parameter has been rescaled from 1 to 4.

| | | 7075-T6 | | 7050-T74 | | 2024-T6 | | 7005-T6 | |
|---|---|---|---|---|---|---|---|---|---|
| | g | p | p·g | p | p·g | p | p·g | p | p·g |
| Density | 9 | 1,46 | 13,14 | 1 | 9 | 2,15 | 19,35 | 4 | 36 |
| Young's Modulus | 6,5 | 3,4 | 22,1 | 3,4 | 22,1 | 4 | 26 | 1 | 6,5 |
| UTS | 6 | 4 | 24 | 3,56 | 21,36 | 2,68 | 16,08 | 1 | 6 |
| Yield Tensile Stress | 8 | 4 | 32 | 3,64 | 29,12 | 2,36 | 18,88 | 1 | 8 |
| Shear Strength | 6 | 4 | 24 | 3,53 | 21,18 | 3,2 | 19,2 | 1 | 6 |
| Elongation at break | 8 | 3 | 24 | 3 | 24 | 1 | 8 | 4 | 32 |
| SUM | 43,5 | | 139,24 | | 126,76 | | 107,51 | | 94,5 |
| OWA | | | 0,8002 | | 0,7285 | | 0,6179 | | 0,5431 |

*Table 11: OWA method for the internal structure.*

The value “g” goes from 0 to 10 and it is the subjective weight given to each parameter that is been analysed since some are more important than others.

With a grade of 0.8, the aluminium 7075-T6 has the most suitable performance according to our OWA process.

The aluminium 7075-T6 has one of the highest strength of the aluminium alloys; however, its resistance to corrosion is also one of the lowest, only above of the cheapest alloys. The 7075-T6 has a composition of 90% Al, 0.2% Cr, 1.7% Cu, 2.6% Mg, 0.5% Fe and 5% Zn generally.

Regarding the skin:

| | | 2024-T3 | | 6061-T6 | | CFRP | | 7075-T6 | |
|---|---|---|---|---|---|---|---|---|---|
| | g | p | p·g | p | p·g | p | p·g | p | p·g |
| Density | 9 | 1,05 | 9,45 | 1,25 | 11,25 | 4 | 36 | 1 | 9 |
| Young's Modulus | 6,5 | 4 | 26 | 1 | 6,5 | 1,79 | 11,635 | 3,5 | 22,75 |
| UTS | 6 | 2,81 | 16,86 | 1 | 6 | 4 | 24 | 2,78 | 16,68 |
| Yield Tensile Stress | 7 | 3 | 21 | 2 | 14 | 1 | 7 | 4 | 28 |
| Shear Strength | 8 | 3,9 | 31,2 | 2,8 | 22,4 | 1 | 8 | 4 | 32 |
| Elongation at break | 8 | 4 | 32 | 2,95 | 23,6 | 1 | 8 | 3,12 | 24,96 |
| SUM | 44,5 | | 136,51 | | 83,75 | | 94,635 | | 133,39 |
| OWA | | | 0,7669 | | 0,4705 | | 0,5317 | | 0,7494 |

*Table 12: OWA method for the skin.*

The methodology is the same as the OWA done for the internal structure choice. The parameter “g” is the subjective value that allows us to rate each parameter and “p” is escalated from 1 to 4 once again. The results of this OWA are not so clear since the winner has a minimum advantage over the second place alloy.

It is important to notice that not all the materials used on this OWA are aluminium alloys, the CFRP which stands for Carbon Fiber Reinforced Polymer are commonly used on nowadays commercial aviation due to their low density and high strength.

The material that will be used for the skin is going to be the 2024-T3 as winner of the OWA shown above.

The differences between both OWA rely on the shear strength. The skin is generally under a higher transversal stress than the internal structure, which has to have a higher resistance over normal loads and bending and torque moment.

## 3.5. Wing design

### 3.5.1. Wing loads

First step is to calculate the wing loads distribution taking into account all the aerodynamic and geometric parameters obtained in the other sections.

From the aerodynamic analysis, the local lift distribution along the span has been obtained using the XFLR5 software.

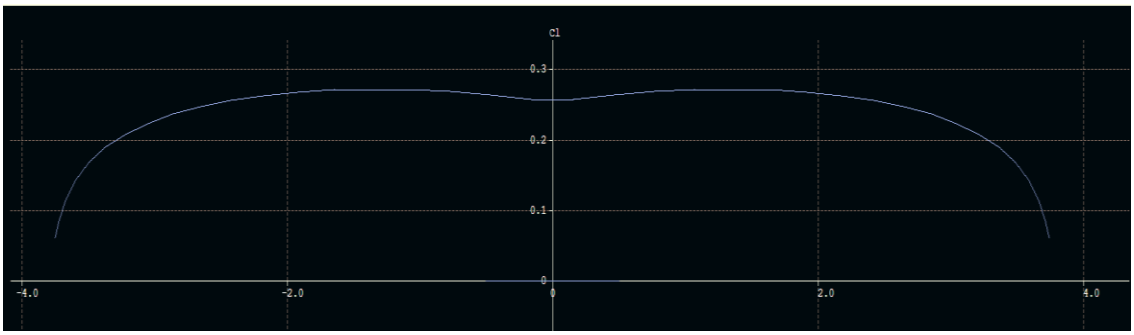


*Figure 14: Local lift distribution along the span.*

In order to ease the calculations, the local lift model has been simplified using linear mathematical equations. Furthermore, since the aerodynamic software does not take into account the interference of the fuselage, a coefficient has been applied on the lift generated near the centre.

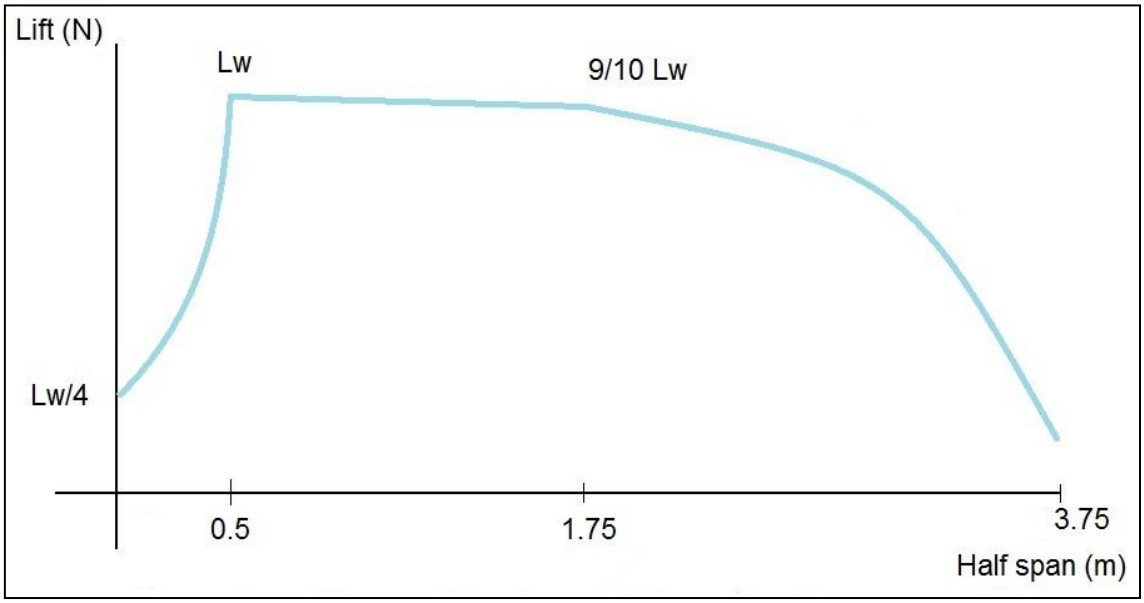


*Figure 15: Local lift distribution used on the analysis.*

The maximum lift ($L_w$) is calculated by the following equation:

$$MTOW \cdot g \cdot n_{max} = 2\left(\frac{L_w}{4} \cdot \frac{0.5}{2} + \frac{\left(L_w + \frac{9}{10}L_w\right)}{2} \cdot \frac{1.25}{2} + \frac{\left(\frac{9}{10}L_w + \frac{2}{10}L_w\right)}{2} \cdot \frac{2}{2}\right) \quad (29)$$

This equation approximates the lift created by the wing by doing the average $L_w$ between each extreme of the section and pondering it by the distance that it occupies.

Solving the equation for $L_w$ replacing MTOW for 460kg, g for 9.81 m/s$^2$ and $n_{max} = 3$:

$$L_w = 5604\ Nm$$

Once the lift per unit of length is known, the weight distribution along the span has to be calculated.

Since our wing does not have any fuel tank or engines like the commercial aviation, the weight of the wing has been decided constant along the wing with the landing gear weight near the root.

Once all the loads distributions are calculated, the only remaining step is to determine the sign of each contribution and sum them. The graph obtained after plotting the results on a Microsoft Excel sheet is:

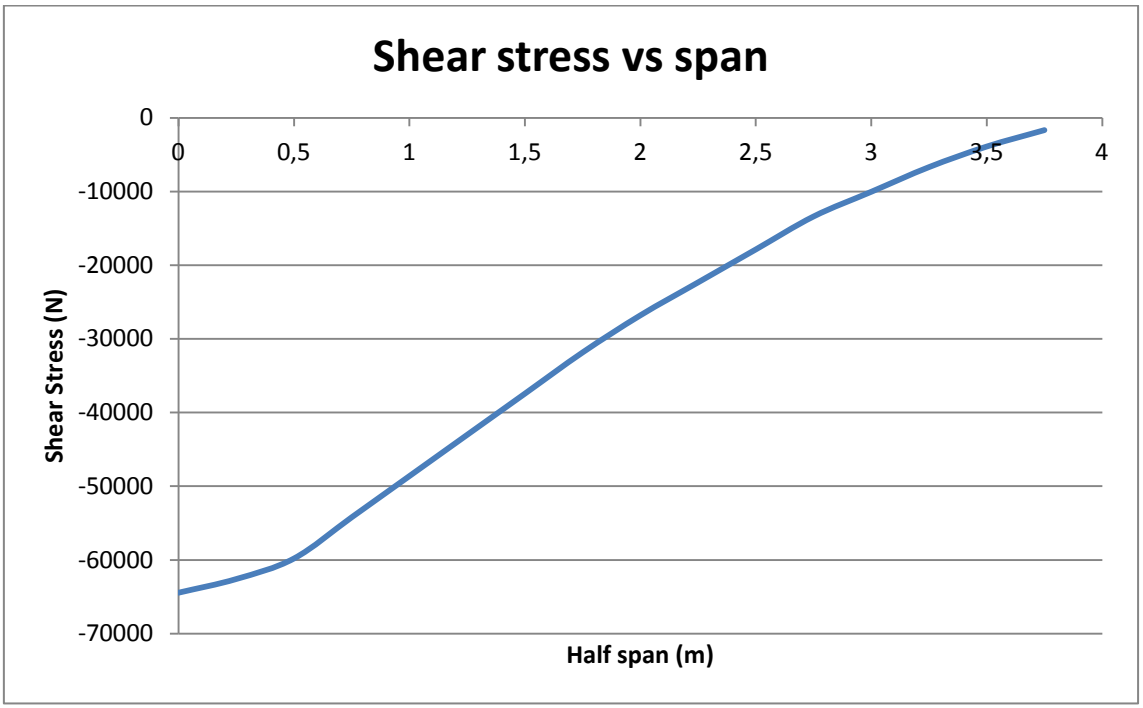


*Figure 16: Shear stress distribution along half of the span.*

Has it can be seen on the graph; the maximum shear stress is achieved on the union fuselage-wing and has an exact value of $-64400N$.

Now, using the values of the shear stress obtained, the bending moment can be obtained by integrating the curve.

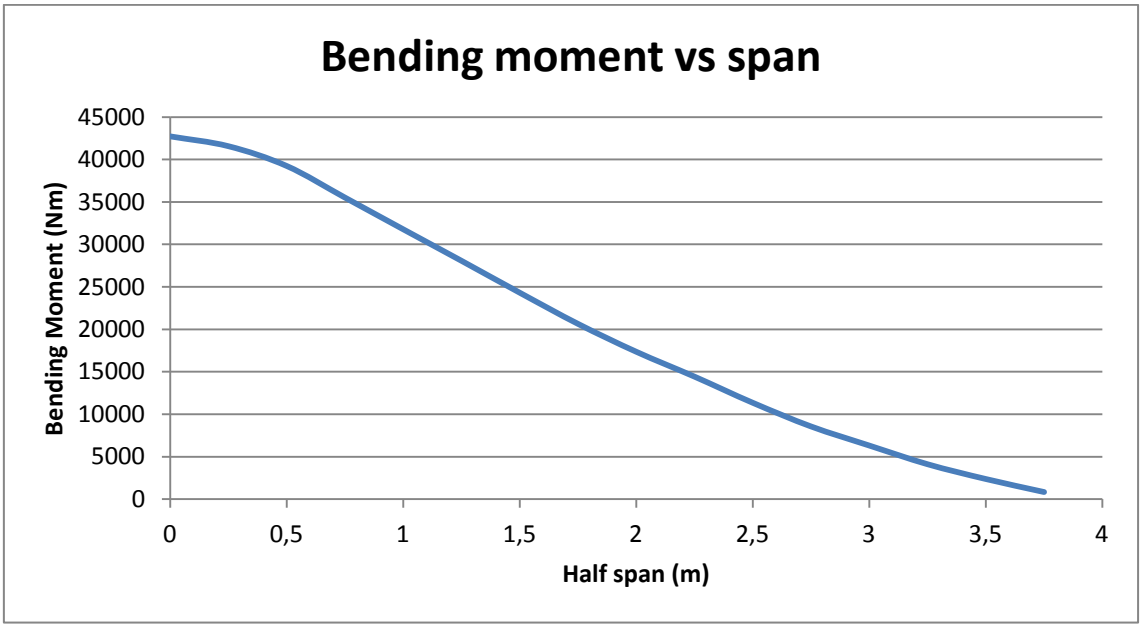


*Figure 17: Bending moment along half of the span.*

Using this local lift distribution simplification and the uniform weight distribution assumption, the final bending moment obtained is:

$$M_{z_{max}} = 42650Nm$$

### 3.5.2. Wing parts

Our UAV will use the same structure used on commercial planes except for the fuel tank, which is not placed on the wings. The main structural elements[17] that have to bear the axial and shear stress and bending and torque moments are:

- Skin.
- Stringers.
- Ribs.
- Spars.

The next image is presented in order to locate each component on the wing.

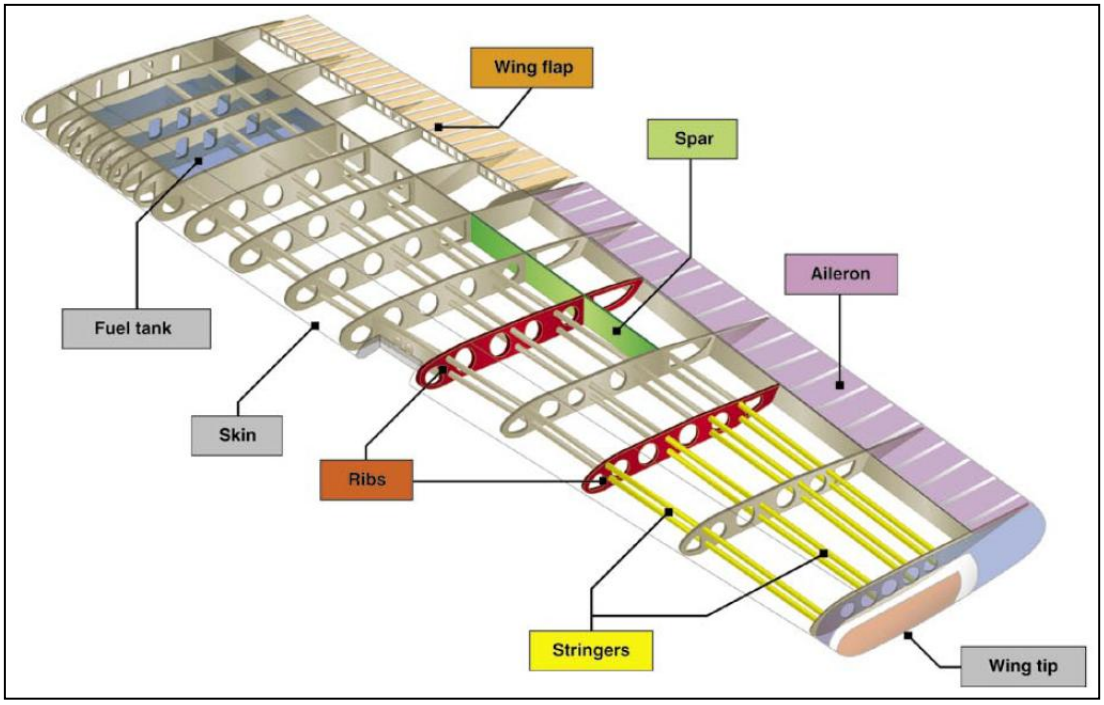


*Figure 18: Structural wing elements of a commercial plane.*

### 3.5.3. Wing box sizing

#### *3.5.3.1. Wing box elements*

Those four elements mentioned above are the components of the wing box. Each one has a specific role on the wing[18].

The skin has mainly three functions:

1) Converts the aerodynamic pressure to transverse shear and transfers it to the adjacent stringers.
2) Resists the wing torque moment.
3) Resists the bending moment created by the axial loads.

The skin thickness is determined by the last two functionalities.

The stringers are used for:

1) Transferring the transverse shear received from the skin to the ribs.
2) Improving skin stability acting as stiffening members.
3) Resist the bending moment generated by axial loads on the wing.

The last function is the most important of the three. Thus, it defines the stringer geometry.

The ribs are made of three components, the web, the caps and vertical stiffeners. Their functions are:

1) The web transfers the point loads received from stringers to the wing spars.
2) Redistribute the torque moment to the spars webs and wing skin.
3) Improving skin stability acting as stiffening members.
4) The vertical stiffeners resist the axial load between the upper and lower wing planks due to compression.

The spars are made of the web and the caps. Its functionalities are:

1) The web resists the wing vertical shear.
2) Resists the wing toque.
3) The caps resist the wing bending moment created by the axial loads.

*3.5.3.2. Simplification model*

The calculations to size the wing box using analytical methods are too difficult to be solved unless some simplifications are applied[19,20].

The first step is to make an equivalence of the airfoil's geometry:

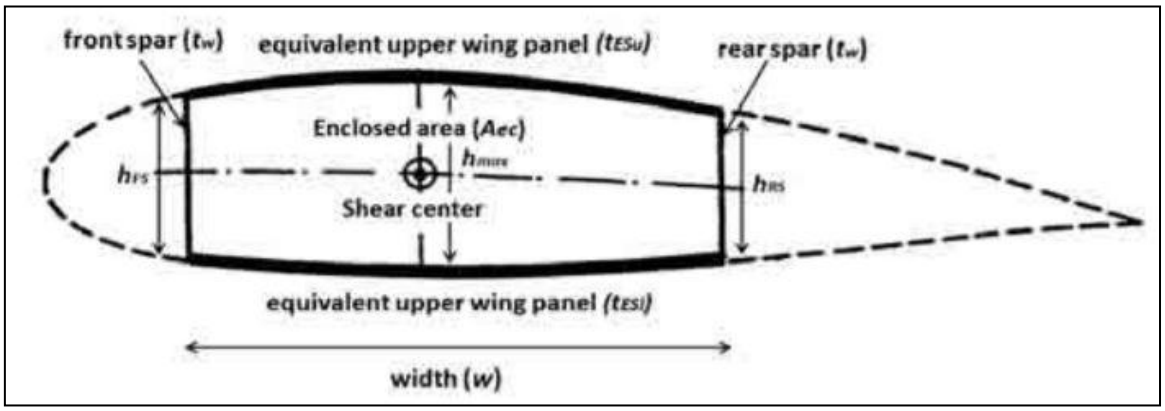


*Figure 19: First approach to wing box structure.*

The model shown above takes into account some simplifications used in order to ease the wing box calculations. However, those simplifications are not

enough to solve the problem by analytical methods. Thus, the new figure goes even further:

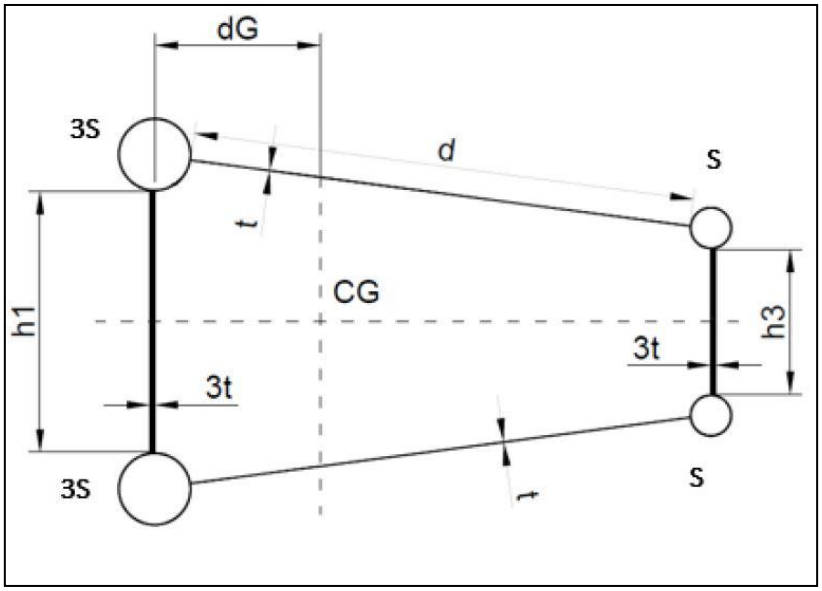


*Figure 20: Wing box analytical model.*

This model will allow us to calculate the span area, their height and the skin minimum thickness. Now that the method that will be used is fully defined, some geometrical calculations can be performed, such as:

- $h_2$: Horizontal distance between the front spar and the rear spar.
- $h_1$: Height of the front spar.
- $h_3$: Height of the rear spar.
- $d$: Distance between the upper front spar area and the upper rear spar area.

$$h_1 = c \cdot t_{0.30c} = c \cdot 0.116 \quad (30)$$

$$h_2 = c \cdot (0.65 - 0.30) \quad (31)$$

$$h_3 = c \cdot t_{0.65c} = c \cdot 0.082 \quad (32)$$

$$d = \sqrt{h_2^2 + (\frac{h_1 - h_3}{2})^2} \quad (33)$$

In equations (30) and (32), the parameters $t_{0.30c}$ and $t_{0.65c}$ mean the thickness of the airfoil in the position 0.30 and 0.65 of the chord, which depend on the airfoil chosen.

Moving on to the shear produced by the weight and the lift on a closed section, the method used in order to solve that problem consists on a decomposition of the closed section. One closed section with a constant shear flow and an opened one with 3 different flows.

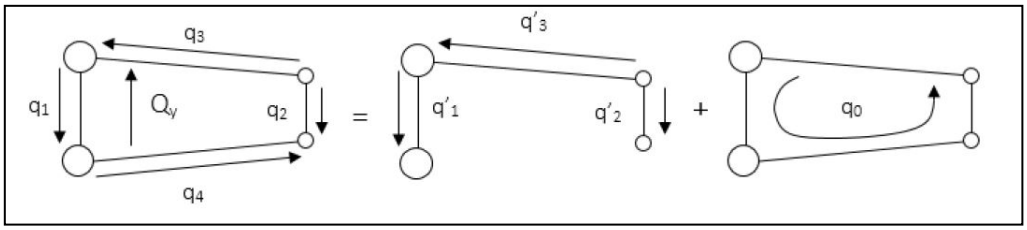


*Figure 21: Shear flow decomposition.*

Open section: Using the equation that relates the jump on shear flow on a node and considering that he node 1 has an open section on one extreme, it is possible to solve $q_1'$:

$$q_1' - q_4' = -\frac{Q_x}{I_y}\sum_{j=1}^{i} x_j S_j - \frac{Q_y}{I_x}\sum_{j=1}^{i} y_j S_j \tag{34}$$

Since $q_4' = 0$ and the coordinate $x = 0$, the equation (34) can be solved as:

$$q_1' = -\frac{Q_y \cdot 3S \cdot (-h_1)}{2 \cdot I_x} \tag{35}$$

There is still one unknown parameter on the equation, the momentum of inertia ($I_x$). It can be solved as:

$$I_x = \int_a^b y^2\, dA = S\left(\frac{3}{2}h_1^2 + \frac{1}{2}h_3^2\right) \tag{36}$$

Since the calculations are made for cruise flight conditions, the aerodynamic drag is cancelled by the thrust. Thus, the horizontal force equals 0.

$$q_3' = 0$$

Only $q_2'$ has to be solved. Applying equilibrium on the section:

$$Q_y = \mathrm{q}_1' \mathrm{h}_1 + \mathrm{q}_2' \mathrm{h}_3$$

$$\mathrm{q}_2' = \frac{Q_y - \mathrm{q}_1' \mathrm{h}_1}{\mathrm{h}_3} = Q_y \left(\frac{1}{\mathrm{h}_3} - \frac{3 \cdot S \cdot \mathrm{h}_1^2}{2 \cdot I_x \cdot \mathrm{h}_3}\right) \quad (37)$$

Closed section: The closed section can be easily solved by the following equation:

$$\oint_{\mathrm{a}}^{\mathrm{b}} \frac{\mathrm{q}\, \mathrm{dS}}{\mathrm{Gt}} = 0$$

$$q_0 = \frac{-\mathrm{q}_2' \cdot \frac{\mathrm{h}_3}{3} + \mathrm{q}_1' \cdot \frac{\mathrm{h}_1}{3}}{\left(\frac{\mathrm{h}_1}{3} + \frac{\mathrm{h}_3}{3} + 2d\right)} \quad (38)$$

Open and closed section: Now the only thing left is to sum both contributions on each panel.

$$\mathrm{q}_1 = q_0 + \mathrm{q}_1' \quad (39)$$

$$\mathrm{q}_2 = -q_0 + \mathrm{q}_2' \quad (40)$$

$$\mathrm{q}_3 = q_0 \quad (41)$$

$$\mathrm{q}_4 = q_0 \quad (42)$$

*3.5.3.3. Spars area*

In this section, the calculations to obtain an approximation of the spars area (3S and S) are going to be made. The equation that allows us to calculate S is:

$$\sigma_{\mathrm{z}} = \frac{M_x}{I_x} y - \frac{\mathrm{M_y}}{I_y} x + \frac{N}{S} \quad (43)$$

Now, applying the flight conditions, the equation can be simplified as:

$$\sigma_{\mathrm{z_{adm}}}^{\max} = \frac{M_x^{max}}{I_x} y_{max} \quad (44)$$

Where $I_x = S \cdot \left(\frac{3}{2}\mathrm{h}_1^2 + \frac{1}{2}\mathrm{h}_3^2\right)$.

Now, the equation can be solved for S since all the parameters are known:

- $\sigma_{z_{adm}}^{max}$: Is the ultimate tensile stress (UTS) of the material chosen on the OWA after applying a security coefficient of 1.5.
- $M_x^{max}$: Maximum bending moment obtained on the wing load distribution. Furthermore, it also dictates the critical stress position, in the joint wing-fuselage.
- $y_{max}$: Is the maximum distance from the centre of the spar to one of its ends. Can be calculated as: $y_{max} = {h_1}/{2}$.

The position of each spar in relation with the chord is also an important parameter that has to be decided.

The front spar is going to be placed at 30% of the chord due to the fact that the airfoil Clark Y gets its maximum thickness close to that value, so is where the spar can get the highest height, reducing the area needed.

The rear spar is going to be placed at 65% of the chord due to the fact will allow us to have a higher flap or aileron chord if needed.

In order to ease the explanation of the calculations, the critical point will be explained step by step and the following points will be omitted since it is the same mathematical and algebraic process.

The values known on the wing-fuselage joint are:

$$M_z = 42725 \text{ Nm}$$

$$t_{0.30c} = 0.226$$

$$t_{0.65c} = 0.1564$$

$$c_{root} = 2$$

$$\sigma_{z_{adm}} = 381.33 \text{ MPa}$$

Now, solving equation (44) for S once $I_x$ is replaced:

$$S = \frac{M_x^{max}}{\sigma_{z_{adm}}^{max} \cdot (\frac{3}{2}h_1^2 + \frac{1}{2}h_3^2)} y_{max} \quad (45)$$

$$S = 1.425\text{cm}^2$$

This is the area of one of the ends of the rear spar. If the area wanted is for the front spar, the value obtained is: $3S = 4.275\text{cm}^2$.

If the same process is repeated for each position of the span, the following graph is obtained:

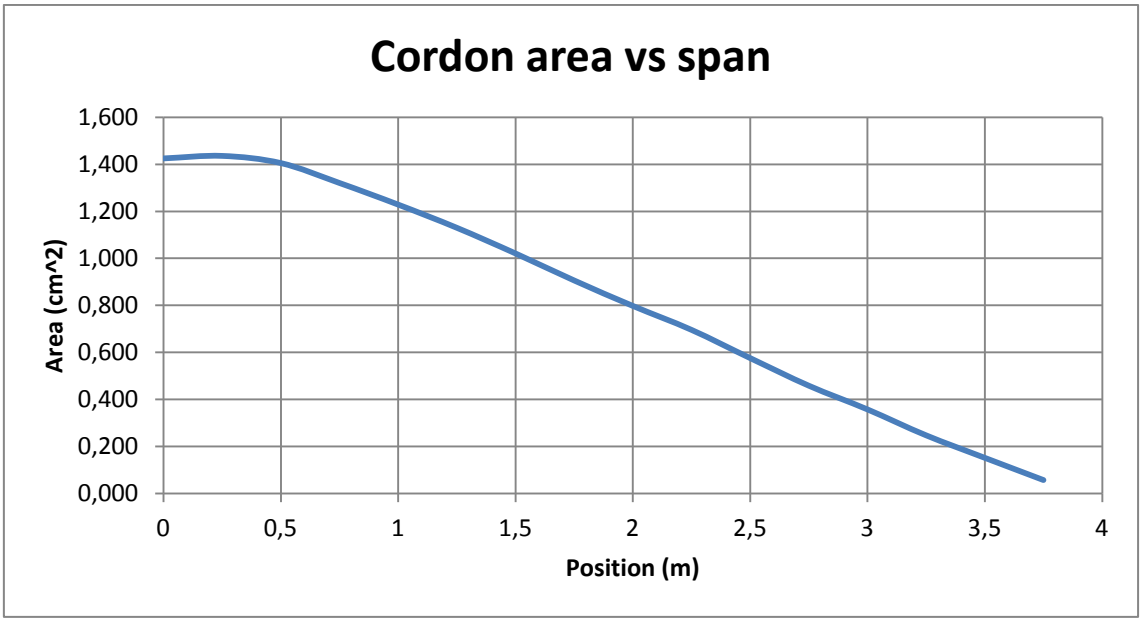


*Figure 22: Rear spar area along half of the span.*

In order to reduce the amount of weight, the optimal choice is to reduce the spar area along the span due to the reduction of the bending moment along the wing.

### *3.5.3.4. Skin thickness*

The skin thickness can be calculated using the following equation:

$$t = \frac{q}{3\tau_{adm}} \quad (46)$$

First of all, the calculation of $\tau_{adm}$ will be done. The material that is going to be used is the aluminium 2024-T3. Knowing that its maximum shear stress has a value of 283MPa and applying a safety coefficient of 1.5:

$$\tau_{adm} = \frac{283}{1.5} = 188.66\text{MPa}$$

The highest shear flow (q) is located on the wing-fuselage joint. This will be the starting point and the example used in order to show the calculation done on each section. Following the simplified model explained above, the parameters needed in order to calculate the skin thickness are:

- The horizontal distance between spars ($h_2$).
- The distance between the upper area of the front spar and the upper area of the rear spar (d).
- The shear stress ($Q_y$).
- The inertia of the spars ( $I_x$).
- Shear flows ($q_1', q_2' \text{ and } q_o$).

The values of the geometrical parameters and the loads applied are:

$$h_2 = 0.156\text{ m}$$

$$d = 0.701\text{m}$$

$$Q_y = 64436\text{N}$$

$$I_x = 0.00014\ m^{-4}$$

Using the equations (35), (37) and (38) the calculations of the shear flow can be performed.

$$q_1' = 245869\text{ N/m}$$

$$q_2' = 56717\text{ N/m}$$

$$q_o = 9155\text{ N/m}$$

Once the three decomposed shear flows are calculated, the next step is to calculate the real shear flow on each panel:

$$q_1 = 255024\text{ N/m}$$

$$q_2 = 47560\text{ N/m}$$

$$q_3 = 9155 \text{N/m}$$

$$q_4 = 9155 \text{ N/m}$$

The shear flow $q_1$ is designed as the critical one due to the fact that it has the highest shear flow.

Going back to equation (46):

$$t = \frac{q}{3\tau_{adm}} = \frac{255024}{3 \cdot 188.66 \cdot 10^6} = 0.00045m = 0.45mm$$

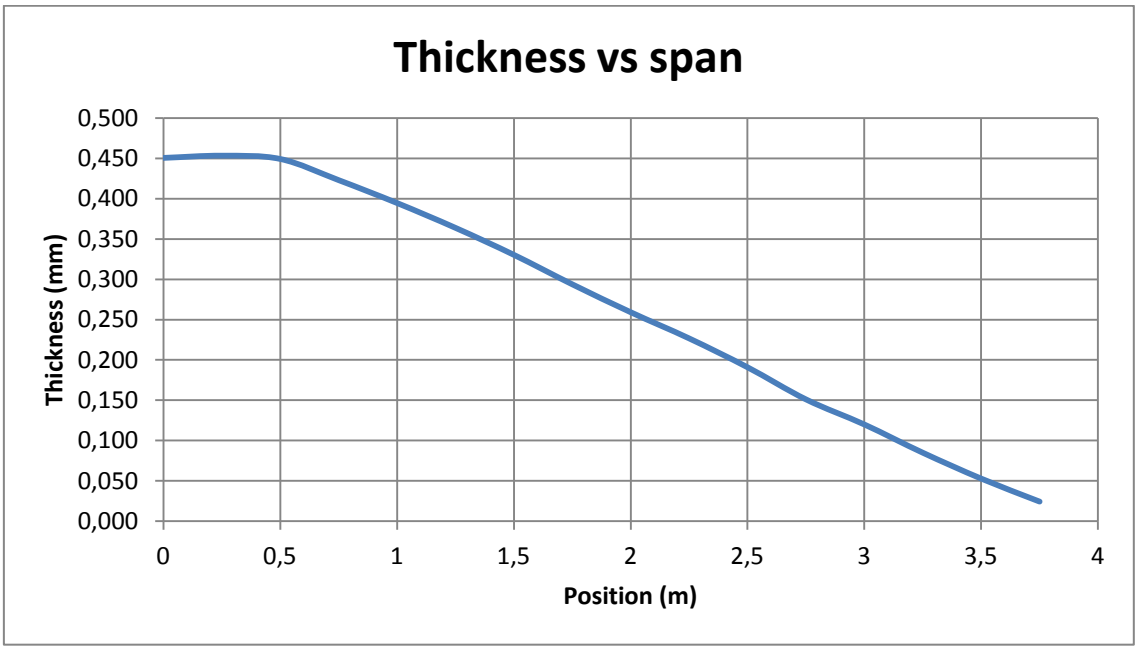


*Figure 23: Skin thickness along half of the span.*

Like the spars area, the thickness of the wing box skin can be reduces along the span due to the decrease of the shear stress along the wing.

### 3.5.4. Spars dimensioning

Now that the parameter "S" and "3S" are known, the selection of what type of cross section is desired.

After retrieving information[21], the selected cross section will be the "I" section due to its advantages.

To totally define this section, 4 parameters are needed.

- h: Total height of the spar.
- b: Width.
- d: Flange thickness.
- t: Spar thickness.

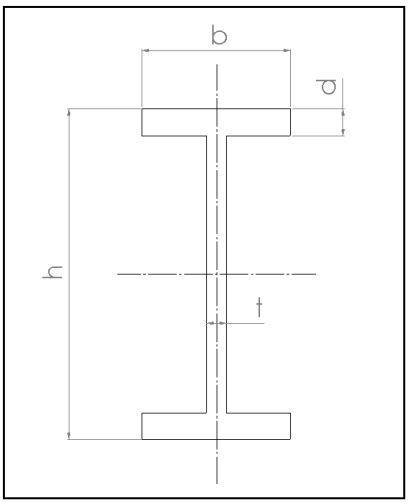


*Figure 24: "I" cross section.*

Due to the fact that the spar area changes along the span, the dimensions will also do it. The following table collects the front spar dimensions:

| h (m) | b (m) | d (m) | t (m) | Upper area ($cm^2$) |
|---|---|---|---|---|
| 0,226 | 0,045 | 0,034 | 0,023 | 15,323 |
| 0,218 | 0,044 | 0,033 | 0,022 | 14,292 |
| 0,211 | 0,042 | 0,032 | 0,021 | 13,298 |
| 0,203 | 0,041 | 0,030 | 0,020 | 12,339 |
| 0,195 | 0,039 | 0,029 | 0,020 | 11,417 |
| 0,187 | 0,037 | 0,028 | 0,019 | 10,530 |
| 0,180 | 0,036 | 0,027 | 0,018 | 9,679 |
| 0,172 | 0,034 | 0,026 | 0,017 | 8,864 |
| 0,164 | 0,033 | 0,025 | 0,016 | 8,084 |
| 0,156 | 0,031 | 0,023 | 0,016 | 7,341 |
| 0,149 | 0,030 | 0,022 | 0,015 | 6,633 |
| 0,141 | 0,028 | 0,021 | 0,014 | 5,961 |
| 0,133 | 0,027 | 0,020 | 0,013 | 5,326 |
| 0,126 | 0,025 | 0,019 | 0,013 | 4,726 |
| 0,118 | 0,024 | 0,018 | 0,012 | 4,161 |
| 0,110 | 0,022 | 0,017 | 0,011 | 3,633 |

*Table 13: Wing's front spar dimensions.*

The upper are is calculated using only “b” and “d” since the theory model places de are “S” and “3S” on the ends of the spar.

Moving on to the rear spar:

| h (m) | b (m) | d (m) | t (m) | Upper area ($cm^2$) |
|---|---|---|---|---|
| 0,156 | 0,031 | 0,023 | 0,016 | 7,34 |
| 0,151 | 0,030 | 0,023 | 0,015 | 6,84 |
| 0,146 | 0,029 | 0,022 | 0,015 | 6,36 |
| 0,140 | 0,028 | 0,021 | 0,014 | 5,89 |
| 0,135 | 0,027 | 0,020 | 0,013 | 5,45 |
| 0,129 | 0,026 | 0,019 | 0,013 | 5,02 |
| 0,124 | 0,025 | 0,019 | 0,012 | 4,61 |
| 0,119 | 0,024 | 0,018 | 0,012 | 4,21 |
| 0,113 | 0,023 | 0,017 | 0,011 | 3,84 |
| 0,108 | 0,022 | 0,016 | 0,011 | 3,48 |
| 0,102 | 0,020 | 0,015 | 0,010 | 3,14 |
| 0,097 | 0,019 | 0,015 | 0,010 | 2,82 |
| 0,091 | 0,018 | 0,014 | 0,009 | 2,51 |
| 0,086 | 0,017 | 0,013 | 0,009 | 2,22 |
| 0,081 | 0,016 | 0,012 | 0,008 | 1,95 |
| 0,075 | 0,015 | 0,011 | 0,008 | 1,70 |

*Table 14: Wing’s rear spar dimensions.*

### 3.5.5. Rib spacing

The rib spacing can be computed by two different methods. The first one is by making use of the equation of critical buckling and solving it for L:

$$\sigma_{z_{adm}}^{max} = \frac{\pi^2 \cdot E \cdot I}{L^2} \tag{47}$$

Where $I$ is the inertia of the section is, $E$ is the Young’s Modulus and $\sigma_{z_{adm}}^{max}$ is the maximum normal stress after using the security coefficient.

The second method is to look for the rib spacing used on commercial and ultra light aviation.

Due to the fact that the first method is quite complicated due to the computation of the airfoil inertia, the second method will be used. Following the theory and the computational study[22], the final rib spacing is decided to be 0.4m since it stabilizes the aluminium wing structure.

### 3.5.6. Computational simulation

Once all the internal structure of the wing is set, the next step is to create a 3D model using all the dimensions obtained on the previous sections.

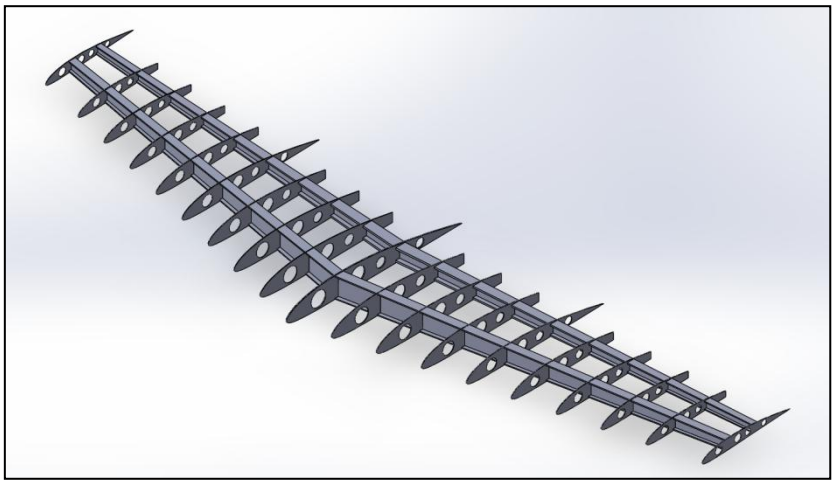

*Figure 25: Wing internal structure.*

As it can be seen, some of the ribs are cut on the last 20% of the chord. That is because both the flap and the ailerons start at that position. Thus, those elements require some manoeuvrability and flexibility since they need to be able to be deflected.

The ribs have been filled with some holes in order to reduce their weight without compromising their structural strength.

The analysis has been performed using the Sold Works simulation software. In order to successfully complete the computational simulation and obtain veridical results, some decisions and points have to be done.

- Material selection: The winner of the OWA for the internal structure has to be selected as the simulation material. That material was the aluminium alloy 7075-T6.
- Space frame: Reducing the space frame's size will result on a more accurate simulation. However, it will also increase the computational time required due to an increase on the number of nodes.
- Supports: In order to do a static analysis, the structure has to be fixed in at least one point. In our case, the section that will act as support is the

rib placed in the fuselage-wing joint. It is represented on the figure as the green arrows.

- Loads distribution: The lift calculated using the local lift distribution is defined as pressure (N/m$^2$) on the lower surface of each spar and it is represented by the arrows displaced bellow the wing. As it can be seen on the figure, the lift distribution is divided into 4 sections (yellow, red, pink and orange). Each one has a different value according to the values obtained on the analytical calculation obtained on the first section of the wing structural design.

Now that all the parameters are chosen, the simulation can be performed:

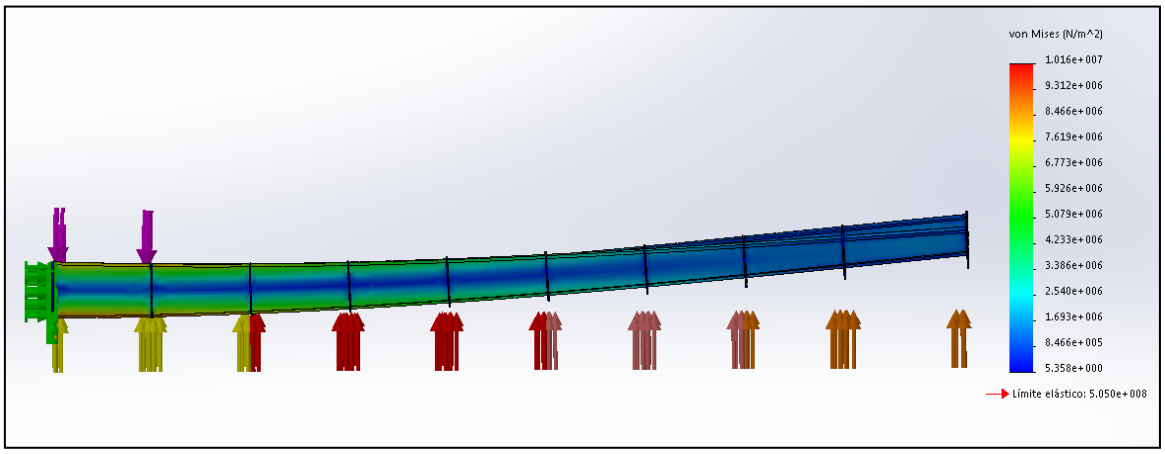


*Figure 26: Von Mises stress analysis.*

As it can be seen on the figure, the maximum Von Mises stress which has a value of $\sigma = 1.01 \cdot 10^7$ does not exceed the elastic limit of the material, which is $UTS = 5{,}05 \cdot 10^8\ MPa$ according to Solid Works material library. Since the calculated stress is lower than the material limit, the design has successfully passed the simulation, always taking into account the entire previous hypothesis made.

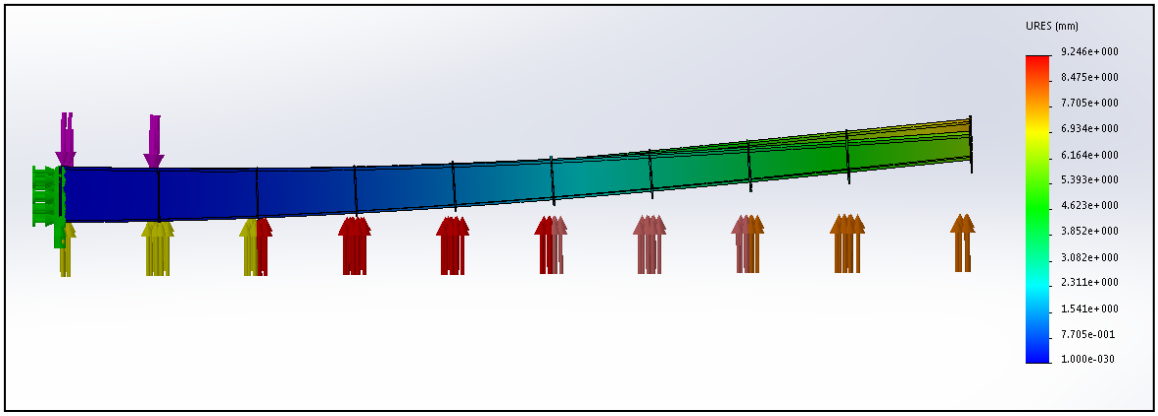


*Figure 27: Displacements distribution along the wing.*

Together with the Von Mises stress, the displacement distribution has been simulated. The highest value obtained is $9.2mm$ on the edge of the wing.

## 3.6. Horizontal stabilizer

The same method used on the wing is going to be applied for the tail internal structure dimensioning.

### 3.6.1. Horizontal stabilizer loads

In order to compute the horizontal stabilizer shear stress and bending moment, the weight and distributions have to be calculated. The software used to calculate the lift is the same program used on the aerodynamic analysis, the XFLR5 free software. The weight has been distributed uniformly along the span.

The maximum shear stress obtained has a value of $-17600N$ and the maximum bending moment $11700Nm$ as it can be seen on the figures obtained after applying a static structural analysis.

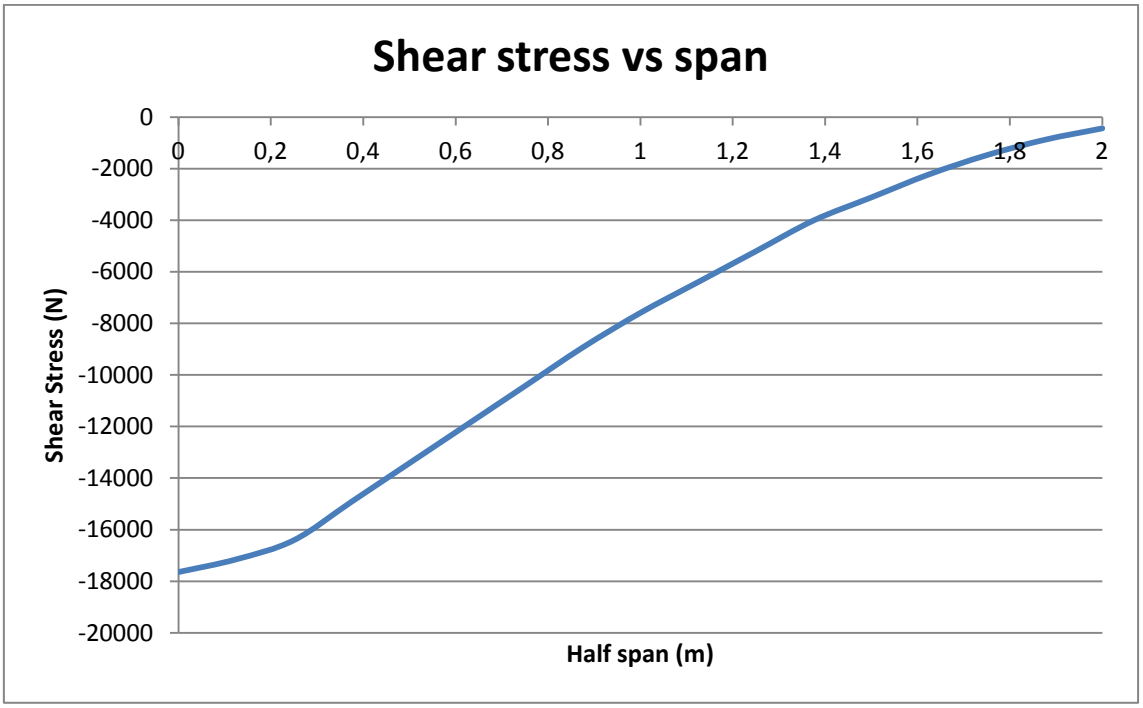


*Figure 28: Shear stress along the horizontal stabilizer.*

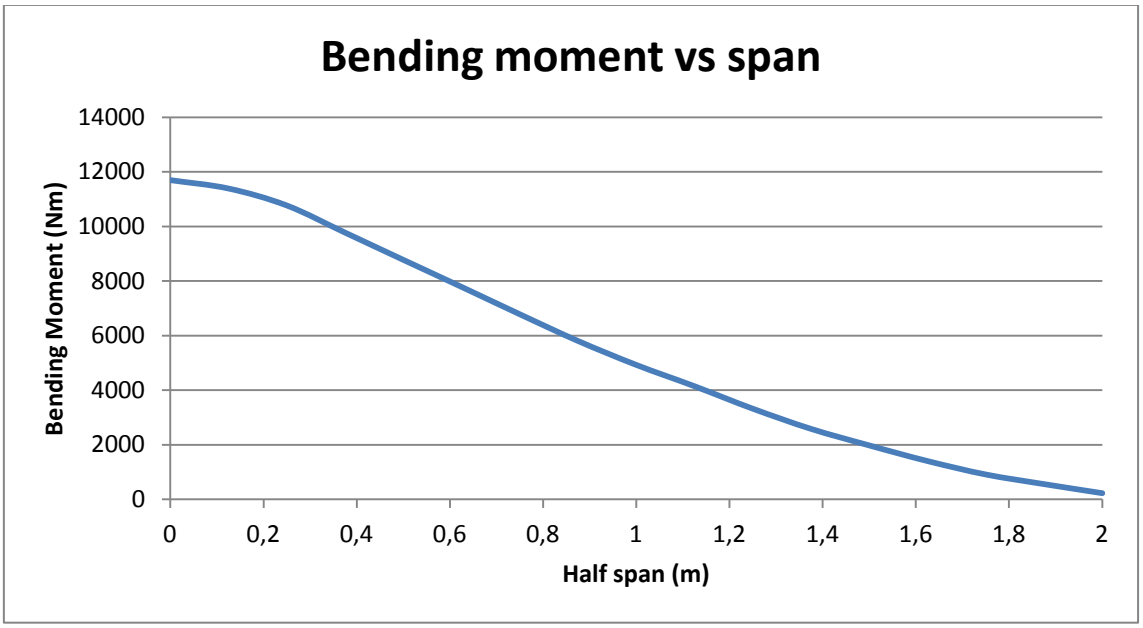


*Figure 29: Bending moment along the horizontal stabilizer.*

### 3.6.2. Spars area

Since the structure of the horizontal stabilizer is equal to the wing, both elements are made of: Ribs, spars, skin and stringers. The same theory and method is used on the horizontal stabilizer. The only differences on the

calculations are the spars heights, the horizontal stabilizer root and tip chord, the span and the bending moment.

After calculation all the equations using Microsoft Excel software, the graph obtained is:

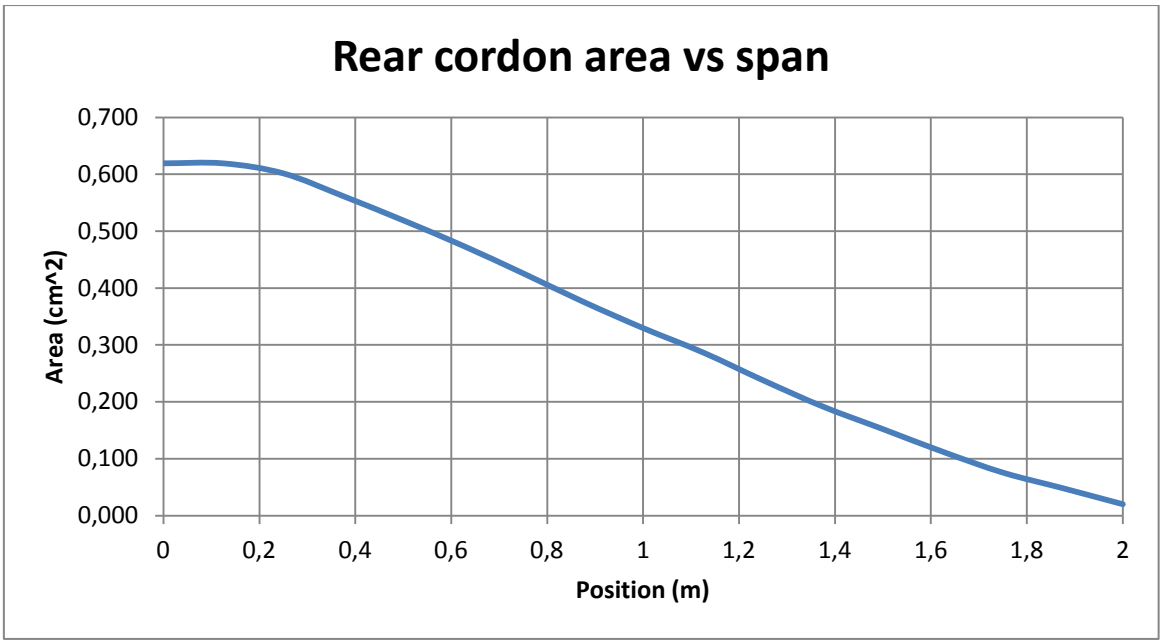


*Figure 30: Rear cordon area along the horizontal stabilizer span.*

As expected, the area decreases along the span. Thus, the spar dimension will also do so in order to reduce the weight on the horizontal stabilizer.

### 3.6.3. Spars dimensioning

The spar section selected for the horizontal stabilizer is the "I" cross section. The parameters that need to be defined are:

- h: Total height of the spar.
- b: Width.
- d: Flange thickness.
- t: Spar thickness.

The following table collects the front spar dimensions. Note that the last column called upper area refers to the area calculated on the previous section. The height and thickness are not used in order to calculate the area "S" because of

the fact that the theory model concentrated all the area on the edges of the spar, thus the area defined by "b" and "d".

| h (m) | b (m) | d (m) | t (m) | Upper Area ($cm^2$) |
|---|---|---|---|---|
| 0,144 | 0,023 | 0,016 | 0,012 | 3,650 |
| 0,140 | 0,022 | 0,015 | 0,011 | 3,462 |
| 0,137 | 0,022 | 0,015 | 0,011 | 3,279 |
| 0,133 | 0,021 | 0,015 | 0,011 | 3,102 |
| 0,129 | 0,021 | 0,014 | 0,010 | 2,929 |
| 0,125 | 0,020 | 0,014 | 0,010 | 2,761 |
| 0,122 | 0,019 | 0,013 | 0,010 | 2,599 |
| 0,118 | 0,019 | 0,013 | 0,009 | 2,441 |
| 0,114 | 0,018 | 0,013 | 0,009 | 2,288 |
| 0,110 | 0,018 | 0,012 | 0,009 | 2,140 |
| 0,107 | 0,017 | 0,012 | 0,009 | 1,997 |
| 0,103 | 0,016 | 0,011 | 0,008 | 1,859 |
| 0,099 | 0,016 | 0,011 | 0,008 | 1,726 |
| 0,095 | 0,015 | 0,010 | 0,008 | 1,598 |
| 0,092 | 0,015 | 0,010 | 0,007 | 1,474 |
| 0,088 | 0,014 | 0,010 | 0,007 | 1,356 |
| 0,084 | 0,013 | 0,009 | 0,007 | 1,243 |

*Table 15: Horizontal stabilizer's front spar dimensions.*

Regarding the rear spar:

| h (m) | b (m) | d (m) | t (m) | Upper Area ($cm^2$) |
|---|---|---|---|---|
| 0,096 | 0,015 | 0,011 | 0,008 | 1,61 |
| 0,093 | 0,015 | 0,010 | 0,007 | 1,53 |
| 0,091 | 0,015 | 0,010 | 0,007 | 1,45 |
| 0,088 | 0,014 | 0,010 | 0,007 | 1,37 |
| 0,086 | 0,014 | 0,009 | 0,007 | 1,29 |
| 0,083 | 0,013 | 0,009 | 0,007 | 1,21 |
| 0,080 | 0,013 | 0,009 | 0,006 | 1,14 |
| 0,078 | 0,012 | 0,009 | 0,006 | 1,07 |
| 0,075 | 0,012 | 0,008 | 0,006 | 1,00 |
| 0,073 | 0,012 | 0,008 | 0,006 | 0,93 |
| 0,070 | 0,011 | 0,008 | 0,006 | 0,87 |
| 0,068 | 0,011 | 0,007 | 0,005 | 0,81 |
| 0,065 | 0,010 | 0,007 | 0,005 | 0,75 |
| 0,063 | 0,010 | 0,007 | 0,005 | 0,69 |
| 0,060 | 0,010 | 0,007 | 0,005 | 0,64 |
| 0,058 | 0,009 | 0,006 | 0,005 | 0,58 |
| 0,055 | 0,009 | 0,006 | 0,004 | 0,53 |

*Table 16: Horizontal stabilizer's rear spar dimensions.*

### 3.6.4. Computational simulation

In order to simulate the internal structure of the horizontal stabilizer, the first requirement is to create a 3D model with the dimensions obtained on the sections above. The software used is the Solid Works.

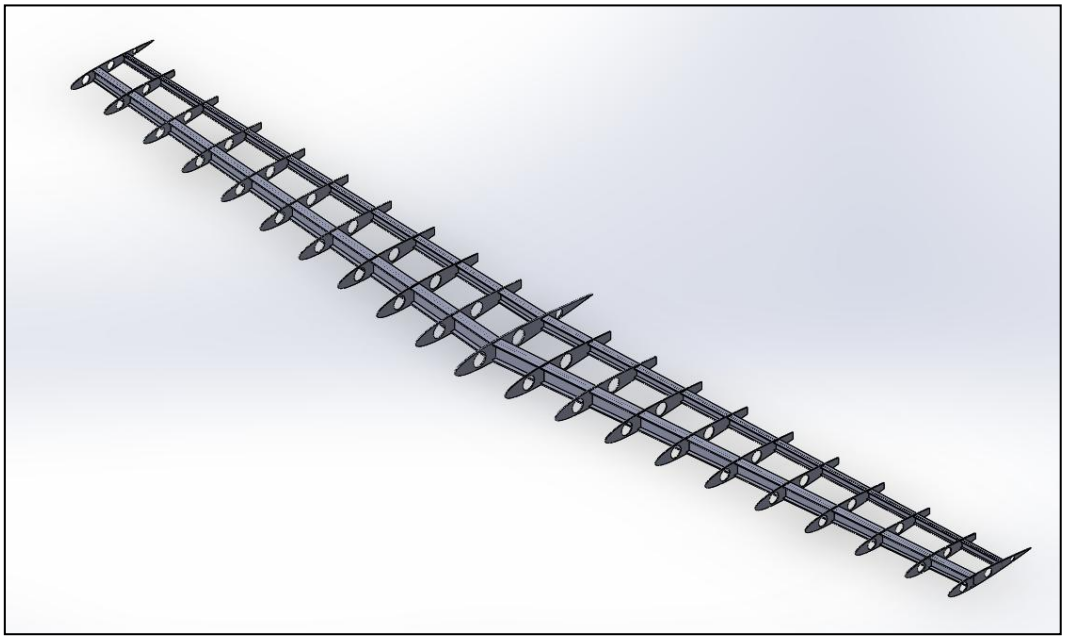

*Figure 31: Horizontal stabilizer's internal structure.*

The ribs have been cut on 20% of the chord due to the elevator. Also, the ribs have some holes in order to reduce the horizontal stabilizer final weight.

Once the 3D model is completed, the next step is to use the Solid Works simulation tool. Before moving on to the results, some elements have to be defined.

- Material: The material used is the same as the wing, the aluminium alloy 7075-T6.
- Support: The fixed support is the closest rib to the fuselage-wing joint. It is represented as green arrows on the figures.
- Space frame: The space frame used is the same as for the wing. The higher number of nodes, the better.
- Loads distribution: As for the wing, the lift distribution has been divided into 4 different sections. The first section has a lower lift value due to the

interference with the fuselage. The second section has the highest value and decreases along with the span due to the chord reduction.

The results obtained are the following:

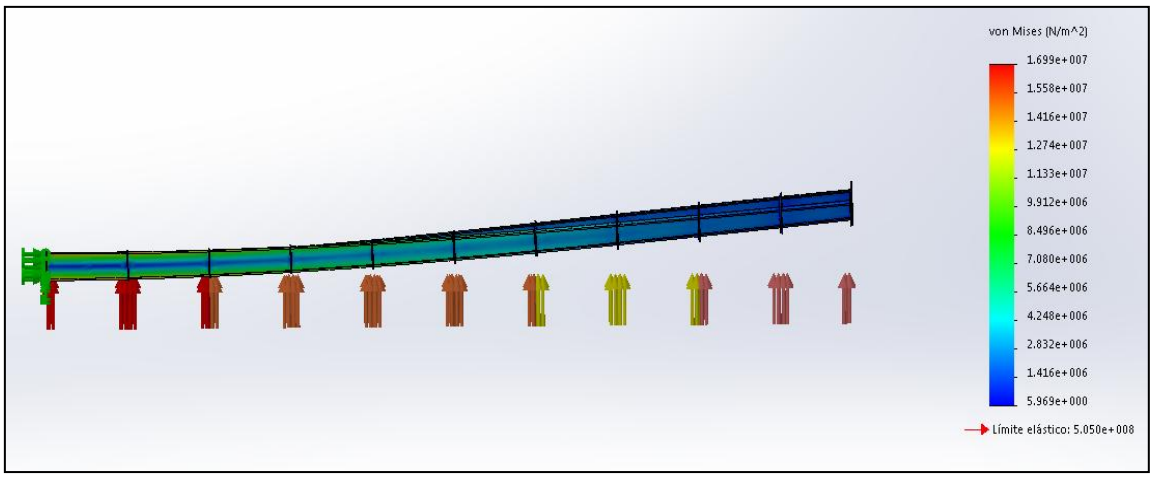


*Figure 32: Horizontal stabilizer's Von Mises simulation.*

As it can be seen on the colour scale, the maximum Von Mises stress does not exceed the elastic limit of the material.

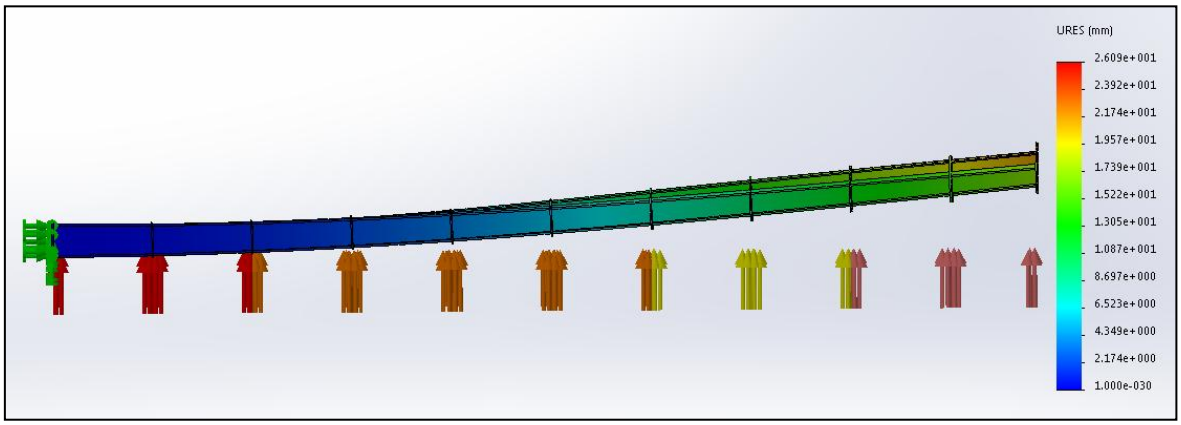


*Figure 33: Horizontal stabilizer's displacements.*

The highest displacement value is obtained on the tip of the horizontal stabilizer and has a value of $26.09mm$.

## 3.7. Landing Gear

Since the landing gear system will be manufactured by an external company, there are a couple of choices that have to be made before finding a manufacturer.

First of all, the landing gear position and configuration have to be selected. Due to our weight distribution and fuselage form, the UAV will have a front wheel and a main landing gear system under the wings. The type of landing gear that will be looked for is called “tricycle”.

Once the landing gear is defined, the next choice is to decide whether the landing gear should be retractable or not. In other words, is worth retracting the landing gear increasing the aerodynamic efficiency in exchange of a higher aircraft weight?

Due to the fact that the endurance of nearly 14 hours is a priority, the answer to the question shown above is yes, the retractable landing gear is worth even though the increase on the aircraft weight and the structural calculations. Furthermore, despite the fact that the non-retractable landing gear may seem to have a better structural analysis, the drag created by the wheels at a medium and high speed can also be a structural difficulty.

The landing gear selected for the UAV is the Lancair’s landing gear system. There is plenty information about the whole kit such as the elements used on the kit and the number of each required[23]. Furthermore, in case that some landing’s gear modifications are needed, the manufacturer can also take personal requests.

The following figure shows an image of Lancair’s landing gear positions and configuration on the Laincair Legacy airplane.


*Figure 34: Lancair's landing gear configuration.*

*Figure 35: Lancair's plane flying with the landing gear retracted.*

# 4. Bibliography

1. UL260i. (2017). Available at: http://ulpower.com/en/engines/ul260/ul260i.
2. UL350iS. (2017). Available at: http://ulpower.com/en/engines/ul350/ul350is#1-specs.
3. Rotax 912 UL/A/F. (2017). Available at: http://www.flyrotax.com/produkte/detail/rotax-912-ul-a-f.html.
4. Airfoil Tools. (2017). Available at: http://airfoiltools.com/search/index.
5. Dadraey, M. in *Aircraft Design: A Systems Engineering Approach* 1–40 (2012).
6. Roskam, J., Tau, C. & Lan, E. Airplane Aerodynamics and Performance. 110 (1997). doi:10.1017/CBO9781107415324.004
7. Rudolph, P. K. C. *High-Lift Systems on Commercial Subsonic Airliners*. *NASA Contractor Report 4746* (1996). doi:NASA CR 4746
8. Raymer, D. P. *Aircraft design: A conceptual approach*. *AIAA Education Series* (2012). doi:http://dx.doi.org/10.2514/4.869112
9. Sadraey, M. H. Tail design. *Aerosp. Ser.* 265–340 (2006). doi:10.1002/9781118352700
10. Sadraey, M. H. Design of control surfaces. *Aerosp. Ser.* 631–753 (2006). doi:10.1002/9781118352700
11. Nicolosi, F., Ciliberti, D. & Della Vecchia, P. *Aerodynamic Design Guidelines of Aircraft Dorsal Fin*. *34th AIAA Applied Aerodynamics Conference* (2016). doi:10.2514/6.2016-4330
12. Roncero, S. E. *Actuaciones Preliminares*.
13. Edwards AFB. *Takeoff & Landing Performance*. *Volume 1 Performance Phase* (1993).
14. Roskam, J. *Airplane Design*. (DARcorporation, 1985).
15. Aluminium Alloys Datasheet. (2017). Available at: http://asm.matweb.com.
16. Composits, A. Mechanical Properties of Carbon Fiber Composite Materials, Fiber / Epoxy resin (120°C Cure). (2014).
17. *Aircraft Structures*. *Aviation Maintenance Technician Handbook - Airframe* **1,** (2012).

18. Wilkinson, R. *Aircraft Structures and Systems*. (MechAero, 2001).
19. Ajaj, R., Smith, D. & Isikveren, A. A conceptual wing-box weight estimation model for transport aircraft. *Aeronaut. J.* **177,** 533–551 (2013).
20. Sedaghati, R. & Mostafa S.A., E. WING – BOX STRUCTURAL DESIGN Wing Rib Stress Analysis and Design Optimization. (2006).
21. Niu, M. C.-Y. *Airframe Structural Design: Practical Design Information and Data on Aircraft Structures*. *GTRI Project A-5636 Technical Report Final Report …* (Hong Kong Conmilit Press, 1988).
22. Arunkumar, K. N., Lohith, N. & Ganesha, B. B. Effect of Ribs and Striner Spacings on the Weight of Aircraft Structure for Aluminium Material. *J. Appl. Sci.* **12,** 1006–1012 (2012).
23. Beringer-aero. (2017). Available at: http://www.beringer-aero.com/en/products/complete-kits-1.htm.